Cell Reports

Article

Repetitive CREB-DNA interactions at gene loci predetermined by CBP induce activity-dependent gene expression in human cortical neurons

Graphical abstract

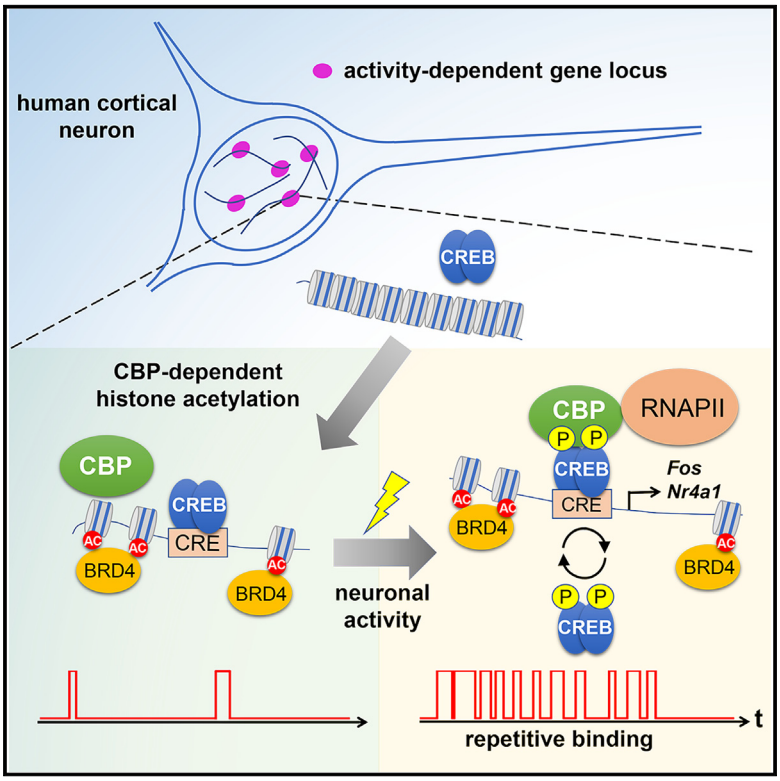

Highlights

- Single-molecule imaging shows CREB and CBP dynamics in human cortical neurons
- Neuronal activity induces CREB-CBP repetitive emergence at histone acetylation sites
- RNAPII accumulates at the repetitive emergence sites, leading to gene expression
- Histone acetylation sites are predetermined by CBP HAT activity

Authors

Yuri Atsumi, Ryohei Iwata, Hiroshi Kimura, Pierre Vanderhaeghen, Nobuhiko Yamamoto, Noriyuki Sugo

Correspondence

nobuhiko@szbl.ac.cn (N.Y.), sugo@fbs.osaka-u.ac.jp (N.S.)

In brief

Atsumi et al. show spatiotemporal dynamics of CREB and CBP in neuronal gene regulation by imaging techniques in human ESC-derived cortical neurons. Histone acetylation is preprepared by CBP at activity-dependent gene loci, while neuronal activity induces gene expression at the acetylation sites by promoting emergence of CREB, CBP, and RNAPII.

Atsumi et al., 2023, Cell Reports ■■, 113576
■■, 2023
https://doi.org/10.1016/j.celrep.2023.113576

CellPress

Cell Reports

CellPress
OPEN ACCESS

Article

Repetitive CREB-DNA interactions at gene loci predetermined by CBP induce activity-dependent gene expression in human cortical neurons

Yuri Atsumi,[1] Ryohei Iwata,[2] Hiroshi Kimura,[3] Pierre Vanderhaeghen,[2] Nobuhiko Yamamoto,[1,4,*] and Noriyuki Sugo[1,5,*]
[1]Graduate School of Frontier Biosciences, Osaka University, Suita, Osaka 565-0871, Japan
[2]VIB-KU Leuven, Center for Brain & Disease Research and KU Leuven, Department of Neurosciences & Leuven Brain Institute, 3000 Leuven, Belgium
[3]Cell Biology Center, Institute of Innovative Research, Tokyo Institute of Technology, Yokohama, Kanagawa 226-8503, Japan
[4]Institute of Neurological and Psychiatric Disorders, Shenzhen Bay Laboratory, Shenzhen, Guangdong 518132, China
[5]Lead contact
*Correspondence: nobuhiko@szbl.ac.cn (N.Y.), sugo@fbs.osaka-u.ac.jp (N.S.)
https://doi.org/10.1016/j.celrep.2023.113576

SUMMARY

Neuronal activity-dependent transcription plays a key role in plasticity and pathology in the brain. An intriguing question is how neuronal activity controls gene expression via interactions of transcription factors with DNA and chromatin modifiers in the nucleus. By utilizing single-molecule imaging in human embryonic stem cell (ESC)-derived cortical neurons, we demonstrate that neuronal activity increases repetitive emergence of cAMP response element-binding protein (CREB) at histone acetylation sites in the nucleus, where RNA polymerase II (RNAPII) accumulation and FOS expression occur rapidly. Neuronal activity also enhances co-localization of CREB and CREB-binding protein (CBP). Increased binding of a constitutively active CREB to CBP efficiently induces CREB repetitive emergence. On the other hand, the formation of histone acetylation sites is dependent on CBP histone modification via acetyltransferase (HAT) activity but is not affected by neuronal activity. Taken together, our results suggest that neuronal activity promotes repetitive CREB-CRE and CREB-CBP interactions at predetermined histone acetylation sites, leading to rapid gene expression.

INTRODUCTION

In the developing brain, sensory-evoked and spontaneous firing activity plays a key role in neuronal circuit remodeling and plasticity by controlling the expression of numerous activity-regulated genes that underlie axon and dendritic growth and synapse formation.[1–4] The impairment of these processes leads to neurodevelopmental and neuropsychiatric disorders, emphasizing their importance for normal acquisition of human cognitive functions.[5–7]

To date, biochemical studies have demonstrated the fundamental molecular mechanisms of activity-dependent gene transcription. Neuronal activity induces calcium influx and activates a subset of transcription factors, thereby regulating the expression of several hundreds of genes positively and negatively with different time courses.[8–14] In particular, cAMP response element-binding protein (CREB) is a well-characterized transcription factor for activity-dependent gene expression. Membrane depolarization induces rapid phosphorylation of CREB and its binding to CRE sequences and initiates transcription accompanied by RNA polymerase II (RNAPII) recruitment.[15–18] An intriguing question is how neuronal activity affects CREB dynamics and induces downstream gene expression spatiotemporally in the nucleus. Indeed, only a subset of CRE sites are transcriptionally activated in an activity-dependent manner,[19] suggesting that CREB binding to selective CRE sites depends on specific regulators.

The epigenetic regulation of chromatin accessibility could modify CREB-dependent transcription.[20,21] CREB-binding protein (CBP) has been shown to contribute to the histone modification via acetyltransferase (HAT) activity that relaxes chromatin structures, followed by recruitment of RNAPII.[22–25] However, the role of CBP in CREB-dependent transcription is not fully uncovered. More specifically, how acetylated regions by CBP are distributed in the nucleus and how CBP interacts with CREB in response to neuronal activity remain unknown.

Here, we attempted to elucidate the spatiotemporal CREB and CBP dynamics in the nucleus, which regulates the expression of activity-dependent genes, using single-molecule imaging (SMI),[26–31] visualization of activated RNAP,[32,33] live imaging of fluorescent-tagged molecules, and mutant overexpression. In particular, SMI is efficient to exhibit spatiotemporal dynamic aspects of transcription factors and chromatin modifiers.[34–39] Moreover, since CBP is a causative gene of Rubinstein-Taybi syndrome, whose patients show mental retardation and intellectual disability,[40–42] we performed these experiments with human embryonic stem cell (ESC)-derived cortical neurons[43,44] in order to link our findings to potential pathophysiological mechanisms.

Please cite this article in press as: Atsumi et al., Repetitive CREB-DNA interactions at gene loci predetermined by CBP induce activity-dependent gene expression in human cortical neurons, Cell Reports (2023), https://doi.org/10.1016/j.celrep.2023.113576

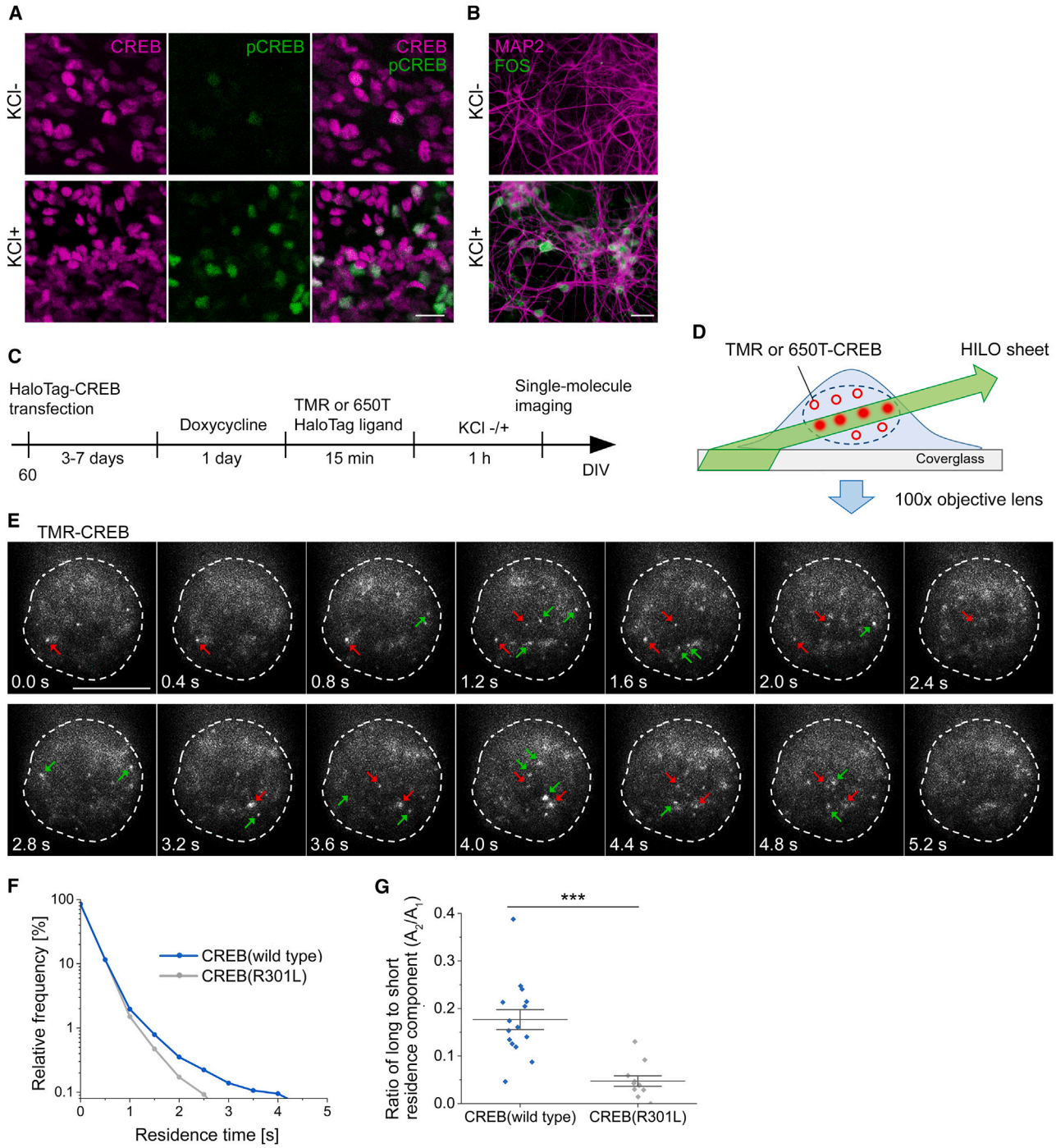

Figure 1. SMI of CREB dynamics in human ESC-derived cortical neurons

(A) Immunocytochemistry for CREB and Ser133 phosphorylated CREB (pCREB) in human ESC-derived cortical neurons at 45 DIV with and without KCl treatment for 30 min.

(B) Immunocytochemistry for FOS in human ESC-derived neurons at 53 DIV with and without KCl treatment. Most cells (86.5%) expressed FOS signals in KCl treatment (n = 104 cells).

(C) Experimental timeline of CREB SMI in human ESC-derived neurons.

(D) Schematic drawing of HILO microscopy for SMI. TMR or 650T-CREB was excited by HILO illumination, and fluorescence images were obtained at the single-molecule level.

(legend continued on next page)

Please cite this article in press as: Atsumi et al., Repetitive CREB-DNA interactions at gene loci predetermined by CBP induce activity-dependent gene expression in human cortical neurons, Cell Reports (2023), https://doi.org/10.1016/j.celrep.2023.113576

Our results demonstrated that neuronal activity induces frequent CREB-DNA and CREB-CBP interactions for several seconds in the nucleus and that the repetitive CREB binding activated the transcription at predetermined histone acetylation sites.

RESULTS

Human ESC-derived cortical neurons respond to neuronal activity

To study activity-dependent CREB dynamics in human cortical neurons, we established an *in vitro* system in which human cortical pyramidal neurons are generated from ESCs and cultured in monolayer so that SMI can be performed.[43] For anterior neural induction, H9 ESCs were first differentiated into neuroepithelial and radial glia cells for 25 days *in vitro* (DIV), followed by differentiation into cortical neurons (Figure S1A). Immunocytochemistry showed that many cells expressed MAP2 and deep-layer neuron markers (TBR1 and CTIP2) about 60 DIV after neural induction (Figure S1B). Up to 90 DIV after neural induction, a small number of cells expressed the upper-layer neuron marker BRN2 and the astrocyte marker GFAP (Figures S1C and S1D). The presynaptic marker VGlut1 and the postsynaptic marker PSD95 were also expressed at the later stages (Figure S1E). These data showed that human ESCs differentiated into cortical neurons according to the order of cortical development, which is consistent with the previous results.[43–45]

To confirm whether neuronal activity induces activity-dependent gene expression in this culture, the expression of activated CREB and its target genes, FOS and NR4A1, was examined in the depolarized condition by increasing extracellular KCl.[46] Immunocytochemistry showed that KCl treatment induced expression of Ser133 phosphorylated CREB and FOS in cultured neurons, while CREB expression was observed regardless of KCl treatment (Figures 1A and 1B). Although the intensities of phosphorylated CREB varied among cells, most cells (86.5%, n = 104 cells) exhibited immunopositive signals in KCl treatment. In addition, RNA fluorescence *in situ* hybridization (FISH) with intron probes and immunocytochemistry with anti-CREB showed that the transcripts of *FOS* and *NR4A1*, but not *GAPDH*, were present at CREB-positive locations in the nucleus of KCl-treated neurons (Figures S1F–S1H). Thus, typical activity-dependent events such as CREB activation and downstream gene expression occurred in human ESC-derived cortical neurons.

SMI demonstrates CREB binding to DNA

To investigate single-molecule CREB dynamics, a Tet-inducible HaloTag-CREB expression vector was transfected with a neuron-specific promoter-driven reporter (pTα1-EGFP) by electroporation in cultured cells at approximately 60 DIV and was visualized by tetramethylrhodamine (TMR) or 650T-conjugated HaloTag ligand (Figure 1C).[30,31] Highly inclined and laminated optical sheet (HILO) illumination (Figure 1D) showed that numerous fluorescent-labeled CREB spots appeared and disappeared in the nucleus of pTα1-EGFP-positive neurons (Figure 1E; Video S1).[47] When CREB spots were subjected to photobleaching under fixation condition, one-stepwise or two-stepwise reduction of fluorescence intensity was found (Figures S2A and S2B), indicating that observed CREB spots are detected at the single-molecule level, as CREB forms a homodimer.[16,31] Moreover, the expression level of HaloTag-CREB was confirmed to be very low compared to the endogenous level (Figures S2C–S2F).

To characterize the CREB dynamics, we measured the residence time of each CREB spot over a 2 min observation period, and the residence time distribution was determined (Figure 1F). While most CREB spots (>90%) disappeared quickly, a small but a significant number of CREB spots resided at the same locations on the order of seconds. We assumed that CREB spots with long residence times might represent specific binding to CRE sites. Indeed, long residence components were markedly reduced when CREB dynamics was examined using mutant CREB (R301L), which lacks DNA binding (Figure 1F).[48] Quantitative analysis further showed that the residence time distribution could be fitted by the sum of two exponential curves with distinct time constants (short and long residence components; Equation 1 in STAR Methods) and that the ratio of the long to short residence component (A_2/A_1) was considerably smaller in CREB (R301L) than in wild-type CREB (0.18 ± 0.02 for wild type, 0.05 ± 0.01 for R301L, $p < 0.001$, Mann-Whitney U test) (Figure 1G; Table S1). This result suggests that CREB spots displaying long residence times represent specific binding to CRE, while CREB spots with short residence times represent non-specific binding to DNA or are free moving. Hereafter, CREB spots with residence times longer than 1 s are referred to as "long-residence CREB spots." Indeed, the exponential component with the short time constant had little contribution to residence time distributions longer than 1 s (see STAR Methods). Furthermore, SMI of CREB in cell-free conditions demonstrated that the same HaloTag-CREB single molecules resided for a long period on the CRE-sequence-containing DNA-coated substratum but not on the κB sequence (Figures S2G and S2H),[30,31] indicating that HaloTag-CREB functions in cultured cells while retaining its sequence-specific binding property.

Neuronal activity increases repetitive appearance of CREB, leading to phosphorylated RNAPII accumulation

Next, we investigated how neuronal activity alters the CREB dynamics. Under 1 h KCl treatment, the residence time distribution of CREB was found to be similar to that without KCl treatment

(E) Representative timelapse images of TMR-CREB in the Tα1-EGFP-positive neuron without KCl treatment. Red arrows indicate TMR-CREB spots that stayed at the same location for longer than 1 s. Green arrows indicate TMR-CREB spots that stayed for less than 1 s. Dashed lines indicate the outline of the nucleus. Scale bar, 10 μm.

(F) The residence time distribution of CREB (wild type) and CREB (R301L). The residence time was significantly shorter in mutant CREB (R301L) than in wild-type CREB (***$p = 6.4 \times 10^{-10}$, Kolmogorov-Smirnov test).

(G) The ratio of long to short residence component (A_2/A_1) was markedly smaller in CREB (R301L) than in wild-type CREB (***$p < 0.001$, Mann-Whitney U test). Mean ± SEM.

In (A) and (B), scale bars, 20 μm. In (F) and (G), n = 15 cells for CREB (wild type) and 11 cells for CREB (R301L).

Please cite this article in press as: Atsumi et al., Repetitive CREB-DNA interactions at gene loci predetermined by CBP induce activity-dependent gene expression in human cortical neurons, Cell Reports (2023), https://doi.org/10.1016/j.celrep.2023.113576

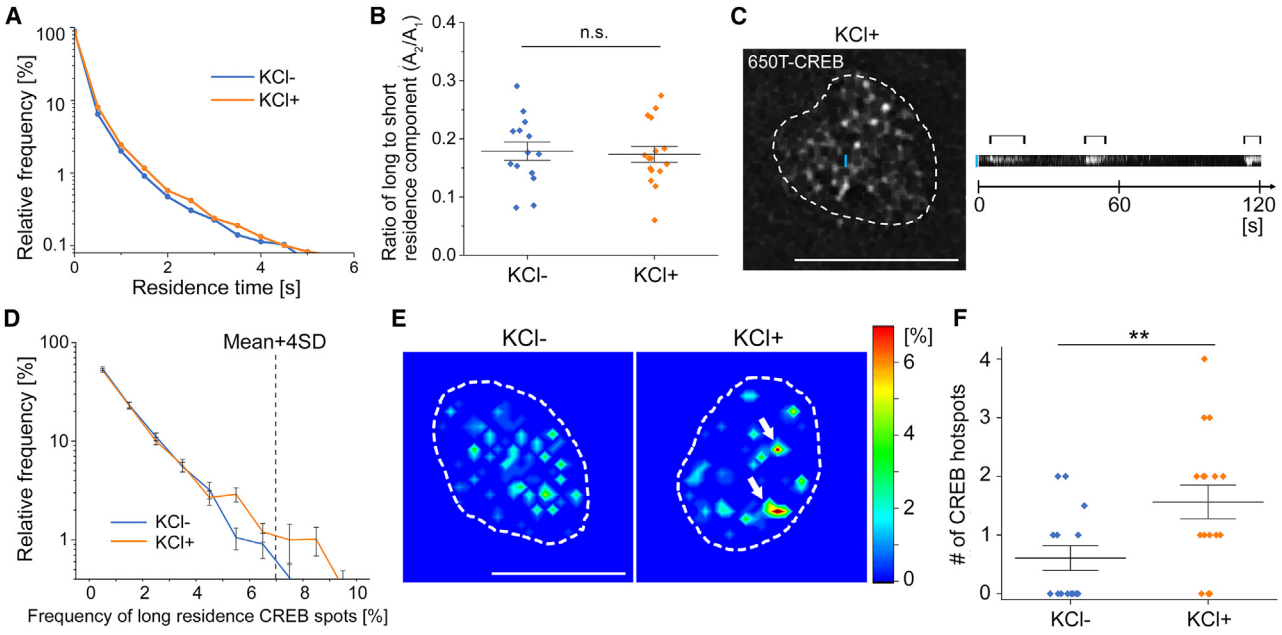

Figure 2. The increase of repetitive CREB emergence at fixed nuclear locations by neuronal stimulation

(A and B) The residence time distribution and A_2/A_1 of CREB were very similar between KCl-untreated and -treated neurons. p = 0.42, Kolmogorov-Smirnov test in (A). p = 0.70, Mann-Whitney U test in (B).

(C) Left, a representative 650T-CREB image in a KCl-treated neuron. Right, the kymograph shows that long-residence CREB spots appeared repeatedly (black brackets) at a restricted location (blue line) of the nucleus during 2 min. The blue line length is 0.8 μm.

(D and E) The area covering the whole nucleus in a neuron was divided into 1,024 (32 × 32) equal micro-domains (0.54 × 0.54 μm). The number of long-residence CREB spots over a 2 min observation period was counted in each micro-domain and divided by the total number of long-residence CREB spots. This value was determined as frequency. The frequency was increased by KCl treatment (D). Color contour maps represent the spatial distribution of the frequency. Two CREB hotspots (>mean + 4 SD, indicated by white arrows) were observed in the KCl-treated neuron, while there was no hotspot in the KCl-untreated neuron.

(F) The number of hotspots was significantly increased by KCl treatment (**p < 0.01, Mann-Whitney U test).

In (A), (B), (D), and (F), n = 14 cells in KCl-untreated neurons and 16 cells for KCl-treated neurons. In (C) and (E), dashed lines represent the perimeter of the nuclei, and scale bars, 10 μm. Mean ± SEM.

(Figure 2A). A_2/A_1 was also unchanged by KCl treatment (0.18 ± 0.02 for KCl−, 0.17 ± 0.01 for KCl+, p = 0.78, Mann-Whitney U test) (Figure 2B; Table S2). Thus, it is unlikely that neuronal activity affects kinetics of individual CREB molecules. However, we found that CREB spots with long residence times appeared repetitively at the same nuclear locations (Figure 2C). In fact, the number of long-residence CREB spots emerging at micro-domains (0.54 × 0.54 μm; see STAR Methods) was increased by KCl treatment (Figure 2D). When the micro-domains with the highly repetitive appearance of long-residence CREB spots were defined as hotspots (>mean + 4 SD; see STAR Methods), the number of hotspots was significantly higher in KCl-treated neurons than in untreated neurons (0.6 ± 0.2 for KCl−, 1.6 ± 0.3 for KCl+, p < 0.01, Mann-Whitney U test) (Figures 2E and 2F; Table S2).

This activity-dependent aspect was also examined in ChR2-expressing cells by applying optogenetic stimulation. Similar to the result of KCl treatment, photostimulation (2 Hz, 5 min) increased the number of hotspots (0.6 ± 0.3 before photostimulation, 1.7 ± 0.3 after photostimulation, p < 0.05, Mann-Whitney U test), while the residence time distribution and A_2/A_1 were not changed (Figure S3; Table S3). Consistent with a previous study in mouse cortical neurons,[31] these results suggest that neuronal activity enhances repetitive CREB-CRE interaction at particular nuclear locations.

Such repetitive emergence of CREB spots may lead to downstream gene expression. To test this possibility, we investigated the spatial relationship between long-residence CREB spots and RNAPII accumulation.[49–51] Since phosphorylated RNAPII works during transcription,[52] a plasmid encoding a GFP-tagged Ser5ph RNAPII-specific probe[32,33] was co-transfected with the HaloTag-CREB expression vector, and then simultaneous live imaging of the RNAPII distribution and single-molecule CREB was performed. RNAPII-GFP signals tended to be overlapped with the locations where long-residence CREB spots appeared repetitively (white arrows in Figure 3A), although the GFP signals were more spread out and broader than those for CREB spots. Moreover, the GFP intensities were increased temporally at the locations where long-residence CREB spots appeared repeatedly, while they were almost unchanged at the sites where long-residence CREB spots scarcely appeared (Figure 3B). The quantitative analysis showed that the time-integral values of the localized GFP signals were well correlated with the number of long-residence CREB spots (Pearson's rank correlation coefficient = 0.87, p = 5.5 × 10^{-13}; see STAR Methods; Figure 3C), suggesting that RNAPII is recruited at nuclear locations where

Please cite this article in press as: Atsumi et al., Repetitive CREB-DNA interactions at gene loci predetermined by CBP induce activity-dependent gene expression in human cortical neurons, Cell Reports (2023), https://doi.org/10.1016/j.celrep.2023.113576

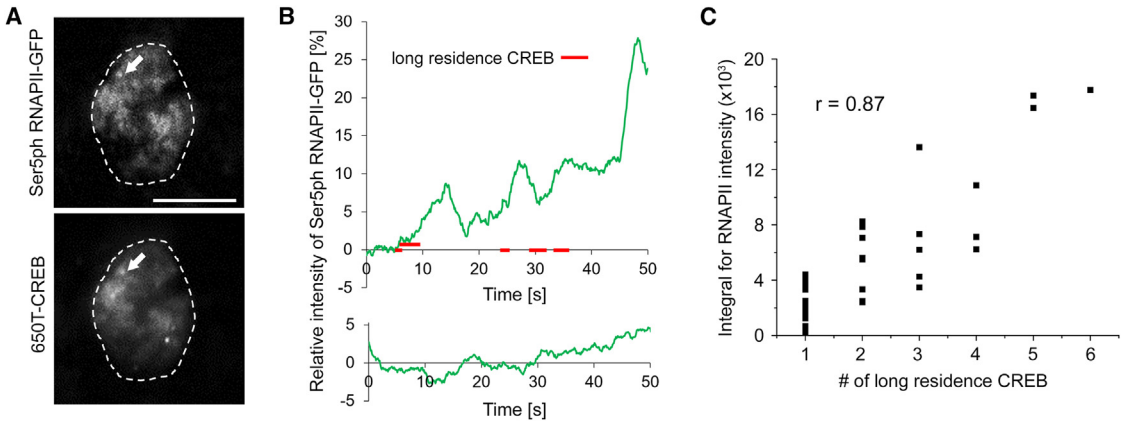

Figure 3. RNAPII accumulation at repetitive CREB-CRE binding sites

(A) Representative images of 650T-CREB and Ser5ph RNAPII-GFP. A 650T-CREB spot co-localized with Ser5ph RNAPII-GFP signals (indicated by white arrows). Dashed lines represent the perimeter of the nuclei. Scale bars, 10 μm.

(B) Representative time courses of Ser5ph RNAPII-GFP intensity and CREB spot appearance at one micro-domain (1.07 × 1.07 μm). Green lines show relative fluorescence intensity of Ser5ph RNAPII-GFP. Red bars show appearance of long-residence CREB spots. RNAPII-GFP signal intensities increased at the micro-domain where long-residence CREB spots appeared repeatedly (upper trace), while the intensities did not change at the micro-domain where no long-residence CREB spots were observed (lower trace).

(C) The number of long-residence CREB spots per micro-domain was strongly correlated with the time-integral values of Ser5ph RNAPII-GFP intensity. Pearson's correlation coefficient: r is 0.87 ($p = 5.5 \times 10^{-13}$ for 40 micro-domains with long-residence CREB spots).

long-residence CREB spots repeatedly appear to induce activity-dependent gene expression.

Activity-dependent repetitive CREB binding promotes transcription at histone acetylation sites

Since histone acetylation contributes to activity-dependent transcription,[21,24] we hypothesized that repetitive CREB-DNA interaction and the subsequent transcription could take place at acetylated chromatin regions. As bromodomain-containing proteins are known to recognize histone acetylation,[53] GFP-tagged bromodomain-containing 4 (BRD4) was used to mark acetylated regions in live imaging of CREB.[54,55]

The spatial relationship between CREB hotspots and BRD4 signals was examined in GFP-BRD4-expressing human cortical cells. For this, a GFP-BRD4 expression plasmid was co-transfected with the HaloTag-CREB plasmid. In the nucleus of cortical neurons, GFP-BRD4 was widely distributed with dotted-like structures. Under KCl treatment, the locations of CREB hotspots were determined by SMI as described above and were compared to GFP-BRD4 spots. As shown in Figure 4A, CREB hotspots tended to appear at GFP-BRD4 spots. The quantitative analysis showed that roughly two-thirds of CREB hotspots co-localized with GFP-BRD4 spots, while randomly distributed nuclear locations exhibited little co-localization ($p < 0.001$, chi-squared test; see STAR Methods; Figures 4B and S4A).

As repetitive CREB binding to DNA would promote downstream gene transcription, the spatial relation was also examined between endogenous BRD4 spots and transcription sites of activity-dependent genes. For this, RNA FISH analysis using intron probes of *FOS* and *NR4A1* was carried out together with immunocytochemistry for BRD4.[9,19] As shown in Figures 4C and 4E, one or two *FOS* and *NR4A1* active transcription sites were detected in KCl-treated neurons, whereas they were hardly detected in KCl-untreated neurons (Figures S4B and S4C). In KCl-treated cultures, these *FOS* spots were often co-localized with BRD4 spots. The analysis of co-localization demonstrated that more than two-thirds of *FOS* transcription sites co-localized with BRD4 spots, significantly higher than if transcription was assumed to occur randomly ($p < 0.001$, chi-squared test; see STAR Methods; Figures 4D and S4D). Similarly, the majority of *NR4A1* transcription sites were co-localized with BRD4 signals in KCl-treated neurons, and the ratio was also significantly higher than the randomized condition ($p < 0.01$, chi-squared test; Figures 4F and S4E). These results imply that repetitive CREB binding to CRE promotes transcription of the early response genes at histone acetylation sites.

CBP HAT activity is essential for CREB-DNA binding

The next question is what activity produces these acetylated sites recognized by BRD4. As HAT activity of CBP may be involved in CREB-dependent transcription,[23] the involvement was examined by inhibiting CBP HAT activity. After overexpression of EGFP-tagged mutant CBP lacking HAT activity (dHAT CBP) (Figure 5A),[56] immunocytochemistry with anti-BRD4 showed that BRD4 signals were rather weak in dHAT-CBP-expressing neurons (Figures 5B and 5C). Quantitative analysis showed that the number of BRD4 spots was significantly decreased by dHAT CBP expression (50.5 ± 2.8 for control, 29.3 ± 1.7 for dHAT CBP, $p < 0.001$, one-way ANOVA with Tukey Kramer test) (Figure 5D). The total volume of BRD4 spots was also significantly smaller in dHAT-CBP-expressing neurons (Figure S5A).

The effect of dHAT CBP on histone acetylation sites was also investigated by histone H4 acetylation (H4ac), as BRD4 may not localize in all of the acetylated sites. Immunocytochemistry with anti-H4ac (K5, -8, -12, and -16) showed that H4ac was also distributed in a dotted manner in the nucleus and that *FOS* transcription sites largely co-localized with H4ac spots (Figures S5B–S5D).

Please cite this article in press as: Atsumi et al., Repetitive CREB-DNA interactions at gene loci predetermined by CBP induce activity-dependent gene expression in human cortical neurons, Cell Reports (2023), https://doi.org/10.1016/j.celrep.2023.113576

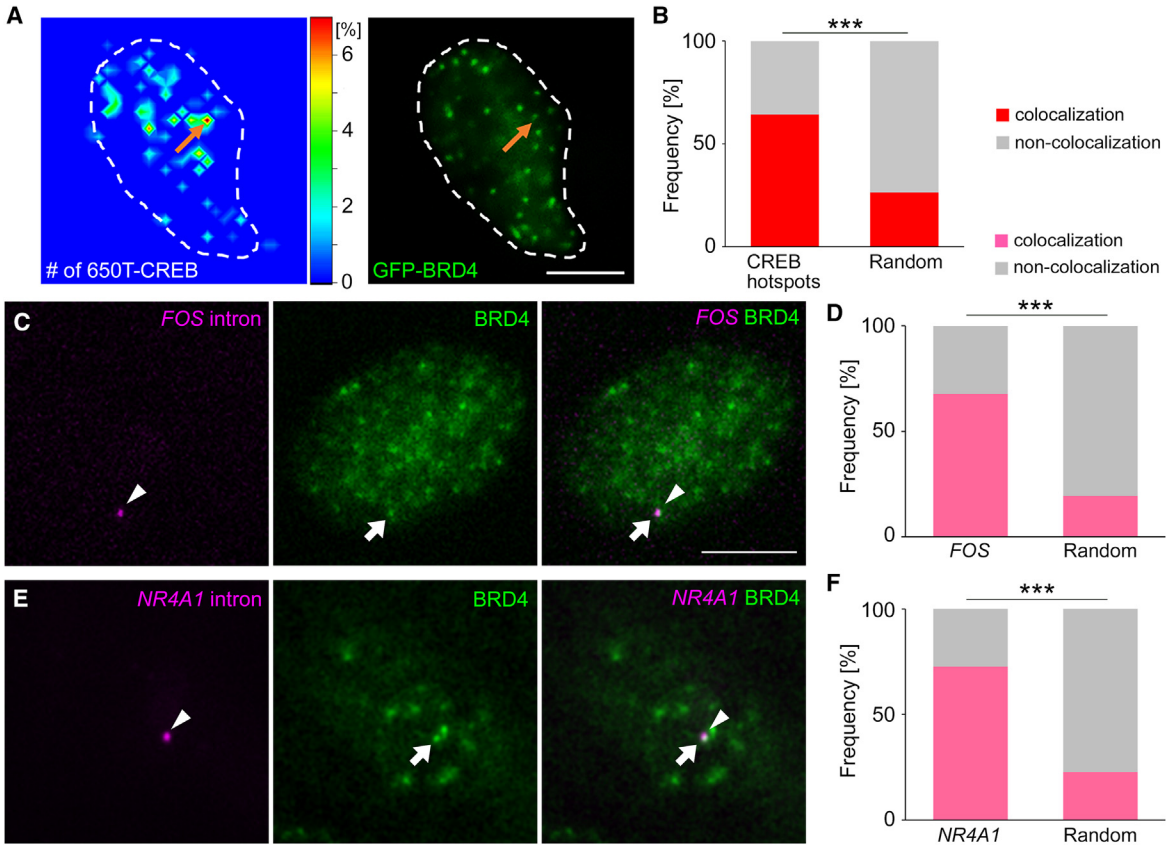

Figure 4. Activity-dependent repetitive CREB-CRE binding and downstream gene transcription at histone acetylation sites

(A) Similar to Figure 2E, the number of CREB spots over a 2 min observation period was counted in each micro-domain (0.54 × 0.54 μm). Color contour map showing the spatial distribution of the frequency of long-residence CREB appearance having long residence times (left) and GFP-BRD4 (right) in KCl-treated cell. A CREB hotspot co-localized with a BRD4 spot (indicated by orange arrows). Dashed lines represent the perimeter of the nuclei.

(B) The co-localization frequency of CREB hotspots with BRD4 signals was higher than when hotspots were randomly distributed in the nucleus (***$p < 0.001$, Mann-Whitney U test, n = 259 spots of 10 cells).

(C and E) Active transcription sites of *FOS* (C) and *NR4A1* (E) co-localized with BRD4 spots (indicated by arrows) in 30 min KCl treatment. Active transcription sites were indicated by arrowheads.

(D and F) The co-localization frequency of active transcription sites with BRD4 spots was significantly higher than the cases where the transcription sites were distributed randomly (***$p < 0.001$, chi-squared test, n = 31 alleles for *FOS* and 22 alleles for *NR4A1*).

In (A), (C), and (E), scale bars, 5 μm.

Thus, H4ac sites are also likely involved in activity-dependent gene expression. In dHAT-CBP-expressing cells, the number of H4ac spots was significantly smaller than control cells (46.8 ± 2.4 for control, 30.3 ± 2.2 for dHAT CBP, $p < 0.001$, one-way ANOVA with Tukey Kramer test) (Figures 5E and 5F), which is similar to the effect on BRD4 spots. These results indicate that the formation of histone acetylation sites in the nucleus strongly depends on CBP HAT activity.

The influence of neuronal activity on formation of acetylation sites was also investigated, as neuronal activity has been reported to modify the histone acetylation level of activity-dependent genes.[21] Unexpectedly, the number of BRD4 spots was not changed by KCl treatment in control cells ($p = 0.70$, 50.5 ± 2.8 for KCl−, 46.4 ± 2.9 for KCl+, one-way ANOVA with Tukey Kramer test) as well as in dHAT-CBP-expressing cells ($p = 0.052$, 29.3 ± 1.7 for KCl−, 38.7 ± 2.8 for KCl+, one-way ANOVA with Tukey Kramer test) (Figures 5C and 5D). The total BRD4 volume was not also altered by KCl treatment in both control and dHAT-CBP-expressing cells (Figure S5A). Similar to BRD4, the number of H4ac spots was not changed by KCl treatment in both dHAT-CBP-expressing cells ($p = 0.99$, 46.8 ± 2.4 for KCl−, 46.2 ± 2.5 for KCl+, one-way ANOVA with Tukey Kramer test) and control cells ($p = 0.30$, 30.3 ± 2.2 for KCl−, 36.6 ± 3.0 for KCl+, one-way ANOVA with Tukey Kramer test) (Figures 5E and 5F). These data indicate that histone acetylation sites and levels represented by BRD4 and H4ac are likely predetermined in the nuclei regardless of neuronal activity.

Since CBP HAT activity contributes to the formation of BRD4-positive acetylated sites and H4ac sites (Figures 5C–5F), the effect of CBP HAT activity on CREB dynamics was also examined. To do this, the Tet-inducible HaloTag-CREB and EGFP-dHAT CBP expression vectors were co-transfected with pTα1-dsRed in cultured cells (Figures 5G and S5E). SMI showed that long-residence CREB spots were markedly decreased in

Please cite this article in press as: Atsumi et al., Repetitive CREB-DNA interactions at gene loci predetermined by CBP induce activity-dependent gene expression in human cortical neurons, Cell Reports (2023), https://doi.org/10.1016/j.celrep.2023.113576

CellPress
OPEN ACCESS

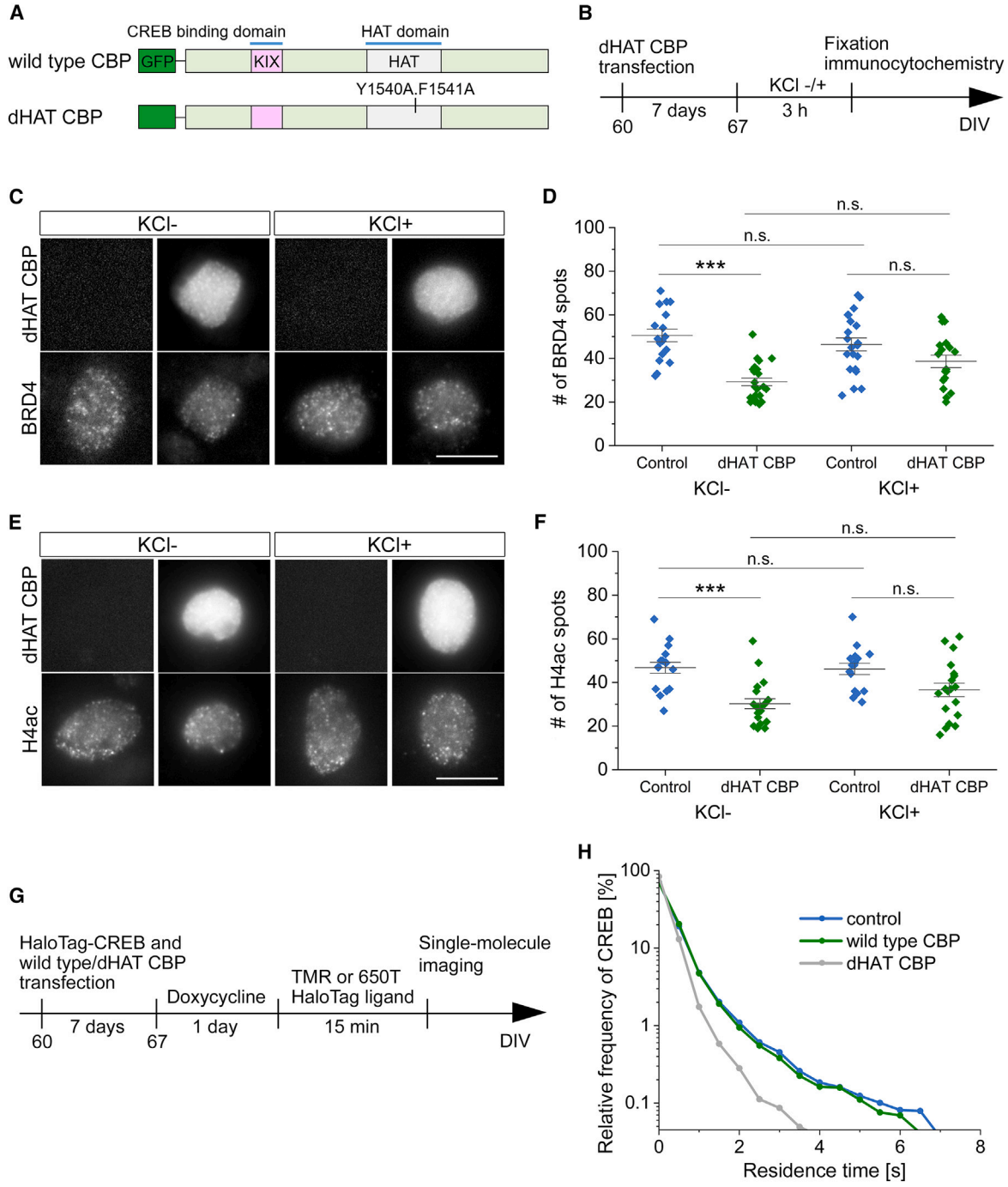

Figure 5. The formation of histone acetylation sites by CBP HAT activity

(A) Human CBP structure and the location of missense mutations (Y1540A.F1541A) in HAT domain.

(B) Experimental timeline of dHAT CBP overexpression.

(C) Representative images of BRD4 signals in dHAT-CBP-positive neurons.

(D) The number of BRD4 spots per cell in dHAT-CBP-expressing neurons was significantly smaller than in control neurons (***$p < 0.001$, one-way ANOVA with Tukey-Kramer post hoc test). On the other hand, regardless of dHAT CBP expression, the number of BRD4 spots did not change under KCl stimulation ($p > 0.05$, one-way ANOVA with Tukey-Kramer post hoc test). n = 17 cells in control neurons, 24 cells in dHAT-CBP-expressing neurons, 21 cells in KCl-treated neurons, and 18 cells in dHAT-CBP-expressing and KCl-treated neurons.

(E) Representative images of H4ac signals in dHAT-CBP-positive neurons.

(F) The number of H4ac spots per cell in dHAT-CBP-expressing neurons was significantly smaller than in control neurons (***$p < 0.001$, one-way ANOVA with Tukey-Kramer post hoc test). On the other hand, regardless of dHAT CBP expression, the number of H4ac spots did not change under KCl stimulation ($p > 0.30$,

(legend continued on next page)

Please cite this article in press as: Atsumi et al., Repetitive CREB-DNA interactions at gene loci predetermined by CBP induce activity-dependent gene expression in human cortical neurons, Cell Reports (2023), https://doi.org/10.1016/j.celrep.2023.113576

dHAT-CBP-expressing neurons, while they were not affected by wild-type CBP overexpression (Figure 5H). Quantitative analysis showed that A_2/A_1 was considerably smaller in dHAT-CBP-expressing neurons than in control and wild-type CBP-expressing neurons ($p < 0.01$, 0.23 ± 0.02 for control, 0.19 ± 0.02 for wild-type CBP, 0.12 ± 0.03 for dHAT CBP, Kruskal-Wallis ANOVA with Dunn's post hoc test) (Table S4). As the frequency of long-residence CREB spots was considerably decreased by dHAT CBP overexpression, the repetitive appearance of CREB spots was also inevitably suppressed. Thus, the formation of acetylated spots was reduced in the absence of CBP HAT activity, which may lead to disruption of CREB-CRE binding. On the other hand, wild-type CBP overexpression did not affect CREB-CRE binding, indicating that endogenous CBP expression is sufficient to generate histone acetylation sites for CREB-CRE binding.

Neuronal activity promotes co-localization of CREB and CBP in the nucleus

To investigate an activity-dependent role of CBP in CREB-CRE binding, the direct interaction of CREB with CBP was investigated by simultaneous SMI of these molecules with different tags and fluorescent dyes.[57,58] HaloTag-CREB and SNAPtag-CBP plasmids were co-transfected in cortical cells and were visualized by TMR-conjugated HaloTag ligand and 647SiR-conjugated SNAPtag ligand, respectively (Figure 6A). CBP spot appearance was also expressed as the sum of two exponential curves with short and long time constants (see Equation 1 and Figure S6). Based on the assumption that the long-residence component represents specific interactions between CBP and other molecules, CBP spots with residence times longer than 0.6 s were selected for analysis (see STAR Methods). As shown in Figure 6B, a CBP spot appeared to overlap with a long-residence CREB spot during the observation. The co-localization was hardly detected under the resting condition, but the frequency of co-localization, which was defined as the ratio of the number of co-localized CREB spots to the total number of long-residence CREB spots, was much enhanced by KCl treatment (0.2 ± 0.2% for KCl−, 4.2 ± 0.8% for KCl+, $p < 0.001$, Kruskal-Wallis ANOVA with Dunn's post hoc test) (Figure 6C).

In contrast, the co-localization frequency of CREB and SNAPtag alone (0.3 ± 0.2% for KCl+) was very low compared to SNAPtag-CBP under KCl stimulation, indicating that a non-specific binding property of SNAPtag does not affect the result.[59,60] Thus, it is likely that neuronal activity promotes CREB-CBP interactions at the single-molecule level.

The temporal features of these spots were further investigated. Interestingly, CREB spots tended to appear earlier than CBP spots. Quantitative analysis showed that long-residence CREB spots emerged significantly earlier than co-localized CBP spots (0.5 ± 0.2 s, $p < 0.05$, one-sample t test against 0), although CREB and CBP spots disappeared at almost the same time (−0.2 ± 0.2 s, $p = 0.29$, one-sample t test against 0) (Figure 6D). This result suggests that CBP binding to CREB follows CREB-CRE binding.

Finally, we investigated the possibility that CBP binding to CREB is essential for CREB repetitive binding, which leads to downstream gene expression. For this, cortical cells were transfected with the constitutively active CREB (CREB Y134F), which accelerates binding to CBP.[61,62] As shown in Figure 6E, the number of hotspots was significantly increased in CREB-Y134F-expressing cells (0.4 ± 0.2 for wild-type CREB, 1.8 ± 0.5 for phosphorylated CREB, $p < 0.05$, Mann-Whitney U test) without elevation of neuronal activity, suggesting that the interaction of CBP with activated CREB is essential for activity-dependent gene expression.

DISCUSSION

In this SMI study, we demonstrated that the elevation of neuronal activity in human cortical neurons increased the frequency of CREB-DNA and CREB-CBP interactions at fixed nuclear locations where activity-dependent gene expression is induced by active RNAPII. Evidence further demonstrated that repetitive CREB appearance and early response gene transcription occurred at BRD4- and H4ac-localized histone acetylation sites, which were produced by CBP HAT activity prior to elevation of neuronal activity. Thus, our results support a model whereby neuronal activity-independent histone acetylation and activity-dependent CREB-DNA and CREB-CBP interactions contribute to regulating gene expression in response to neuronal activity.

Neuronal activity promotes repetitive CREB-DNA binding, leading to early response gene transcription

The present SMI demonstrated that neuronal activity increases repetitive CREB appearance at specific nuclear locations in human cortical neurons without changing the residence time distribution, in accordance with our previous result in CREB dynamics in mouse cortical neurons.[31] Furthermore, RNAPII imaging strongly indicates that repetitive CREB binding to CRE promotes the active transcription of *FOS* and *NR4A1* through rapid RNAPII accumulation. One may think that the total time of CREB binding is more important. However, the fact that neuronal activity did not alter the kinetics of individual CREB molecules suggests that repetitive CREB binding to CRE sites is indispensable for RNAPII accumulation and downstream gene expression. Consistent with this view, fluorescence recovery after photobleaching suggests that transcription factors frequently bind to DNA in response to stimulus signals.[63–65] On the other hand, the individual binding time of serum response factor (SRF) has been reported to increase after stimulation.[29,59] There may be two possible modes of

one-way ANOVA with Tukey-Kramer post hoc test). n = 17 cells in control neurons, 20 cells in dHAT-CBP-expressing neurons, 16 cells in KCl-treated neurons, and 19 cells in dHAT-CBP-expressing and KCl-treated neurons.

(G) Experimental timeline of CREB SMI in dHAT-CBP-expressing neurons.

(H) The residence time of CREB in dHAT-CBP-expressing neurons was markedly shorter than that in EGFP-expressing neurons (***$p = 1.1 \times 10^{-8}$, Kolmogorov-Smirnov test, n = 14 cells in control and 12 cells in dHAT CBP), while the residence time in wild-type CBP-expressing neurons was not affected ($p = 0.81$, Kolmogorov-Smirnov test, n = 10 cells in wild-type CBP).

In (C) and (E), scale bars, 10 μm. Mean ± SEM.

Please cite this article in press as: Atsumi et al., Repetitive CREB-DNA interactions at gene loci predetermined by CBP induce activity-dependent gene expression in human cortical neurons, Cell Reports (2023), https://doi.org/10.1016/j.celrep.2023.113576

CellPress
OPEN ACCESS

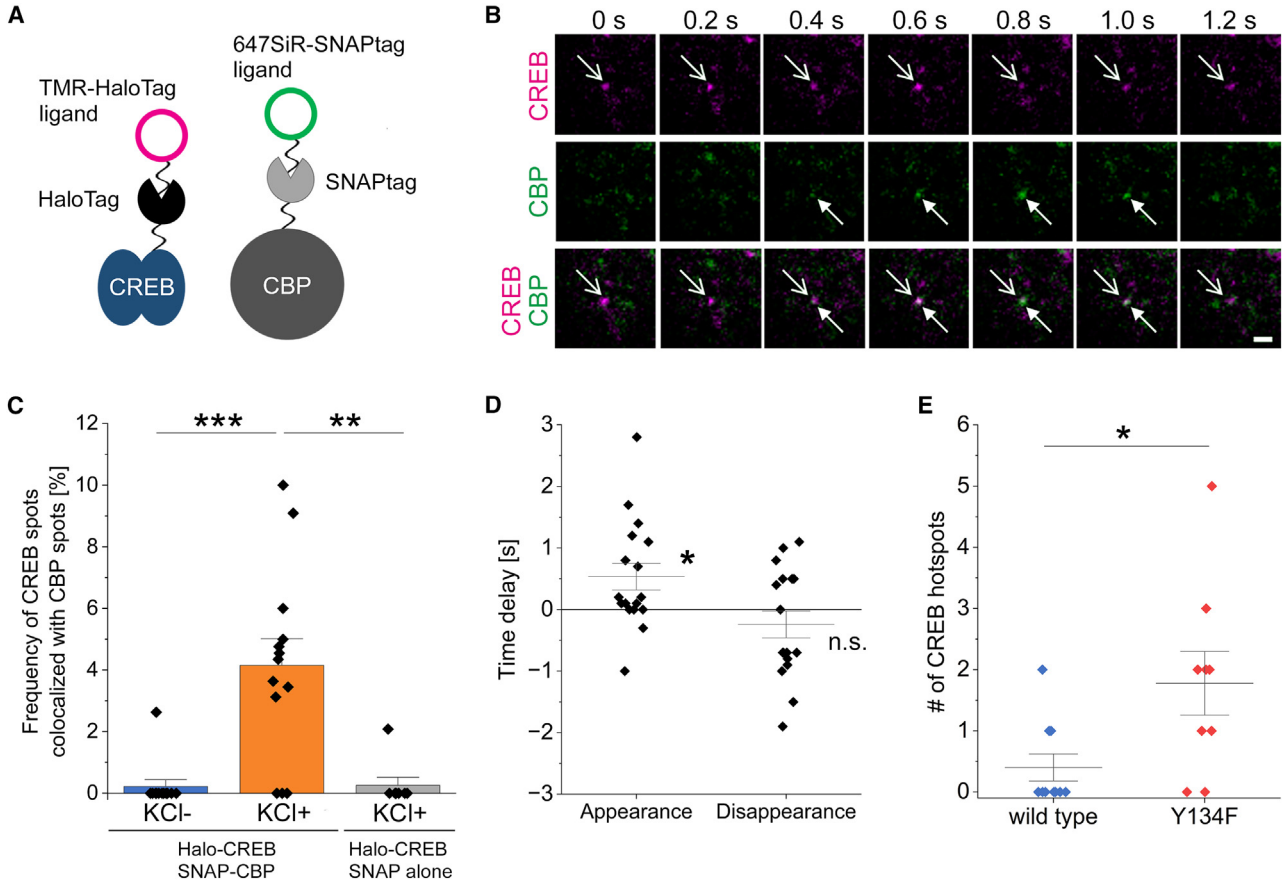

Figure 6. Activity-dependent CREB-CBP interaction at the single-molecule level

(A) Schematic drawing of two-color SMI of HaloTag-CREB and SNAPtag-CBP. TMR-CREB and 647SiR-CBP were visualized simultaneously at the single-molecule level.

(B) A CBP spot co-localized with a CREB spot in the nucleus. These two spots were indicated by white arrows. Scale bar, 1 μm.

(C) The frequency of long-residence CREB spots co-localized with CBP spots (>0.6 s) was much increased by KCl treatment (***$p < 0.001$, Kruskal-Wallis ANOVA with Dunn's post hoc test), whereas the co-localization of CREB and SNAPtag alone was very low compared to SNAPtag-CBP under KCl stimulation (**$p < 0.01$, Kruskal-Wallis ANOVA with Dunn's post hoc test). n = 12 cells in KCl−, 13 cells in KCl+, and 8 cells in SNAPtag-alone KCl+.

(D) Time delays of CBP binding to CREB (appearance) and CBP dissociation from CREB (disappearance) were measured (for 17 spots from 11 cells). CREB spots appearance was earlier than CBP spots (*$p < 0.05$, one-sample t test against 0).

(E) The number of CREB hotspots were compared between HaloTag-CREB (wild type) and CREB (Y134F). The number of CREB hotspots in Y134F was significantly higher than wild type (*$p < 0.05$, Mann-Whitney U test, n = 9 cells for wild type and 9 cells for Y134F). The data of HaloTag-CREB (wild type) were used for Figure S3D.

Mean ± SEM shown in (C) and (D).

interaction between transcription factors and their target DNA for activity-dependent transcription.

Predetermined histone acetylation sites are scaffolds of activity-dependent transcription

It has been shown that histone acetylation sites represented by BRD4 spots are scattered in the nucleus of mouse ESCs.[66] Our imaging study further demonstrated that such acetylated sites are formed for activity-dependent gene expression in postmitotic neurons. We also found that a large population of these acetylated sites are produced by CBP HAT activity and are scattered throughout the nucleus of cortical neurons, although CBP-independent HAT activity may also be involved (Figures 5D and 5F). Moreover, the fact that the number of histone acetylation sites was not changed with neuronal activation suggests that these acetylated sites are predetermined regardless of neuronal activity (Figures 5C–5F). However, the possibility cannot be excluded that neuronal stimulation increases the histone acetylation level at some activity-dependent gene loci since these acetylated sites should contain not only activity-dependent but also cell-type-specific gene loci.[9,21,67] In addition, KCl treatment increased the co-localization of CREB and CBP (Figure 6C), suggesting the importance of neuronal activity-dependent CBP function at the predetermined sites. Neuronal activity has also shown to promote nucleocytoplasmic translocation of histone deacetylation enzymes and induce immediate-early gene expression.[68,69] Removal of deacetylation activity in the nucleus could contribute to appropriate

Please cite this article in press as: Atsumi et al., Repetitive CREB-DNA interactions at gene loci predetermined by CBP induce activity-dependent gene expression in human cortical neurons, Cell Reports (2023), https://doi.org/10.1016/j.celrep.2023.113576

activity-dependent gene expression together with local HAT activity.

The simultaneous measurement of CBP and CREB indicated that neuronal activity enhanced direct CREB-CBP interaction (Figure 6C). Given that CBP promotes RNAPII recruitment and elongation,[70] it is conceivable that direct CBP binding to CREB induces downstream transcription via RNAPII accumulation. This view is also supported by the fact that CBP binding to CREB follows CREB-DNA binding (Figure 6D). In addition to RNAPII recruitment, activity-dependent CBP participation would further increase acetylation levels at predetermined acetylated loci, leading to repetitive CREB binding (Figure 6E) and subsequent RNA synthesis. Such activity-dependent CBP function might contribute to the selection of specific gene loci from a large number of acetylation sites.

Biochemical studies have demonstrated that neuronal activity induces rapid CREB phosphorylation in the nucleus,[11,12] resulting in recruitment of RNAPII by CBP.[16,18,70] The present findings would add the following scenario to the activity-dependent transcription mechanism in terms of spatiotemporal regulation. (1) In the absence of electrical activity, predetermined histone acetylation sites are scattered throughout the nucleus to prepare for transcription of activity-dependent genes. (2) Neuronal activity promotes CBP-CREB interaction and repetitive CREB-CRE binding at the predetermined gene loci. (3) Finally, rapid RNAPII accumulation is induced, and mRNA synthesis of activity-dependent genes such as *FOS* and *NR4A1* is accelerated. We would like to emphasize that histone acetylation predetermined by CBP HAT activity and neuronal activity-dependent CREB-CRE and CBP-CREB binding regulate rapid transcription of specific genes.

Dysregulation of CREB dynamics may be relevant to neurological pathology

Our findings demonstrate that inactivation of CBP HAT leads to disruption of activity-dependent CREB dynamics in human cortical neurons, which could be directly relevant to the disease mechanisms found in Rubinstein-Taybi syndrome or in mouse models. Consistent with this view, induced pluripotent stem cell (iPSC)-derived neurons from patients with Rubinstein-Taybi syndrome have shown impaired neurite outgrowth.[71,72] Abnormalities of gene expression and cognitive functions have also been reported in CBP mutant mice.[73,74]

In accordance with the previous study using mouse cortical neurons,[31] the present study demonstrated that neuronal activity also promotes repetitive CREB-CRE binding in human cortical neurons, suggesting that activity-dependent CREB dynamics is shared across species. However, CREB-CRE binding time (t_2) was shorter in human cortical neurons (compare Tables S2 and S3 in this study with Tables 2 and 3 in the reference paper[31]). This might enable precise gene regulation in human cortical neurons by increasing the temporal resolution. A recent study suggests that human genomic regions showing dynamic changes in human lineage regulate the expression of neurodevelopmental genes.[75] Another genome-wide analysis reported human-specific histone methylation patterns in neuropsychiatric-disease-associated genes.[76] These evolutionary genomic and chromatin structural changes around CRE sequences might contribute to generating the difference in CREB-CRE binding time between human and mouse cortical neurons. Furthermore, as previous studies have demonstrated that neuronal maturation and biochemical reactions including transcription are slower in human,[77–79] it would be interesting to determine whether other temporal aspects in activity-dependent transcription are involved in the plasticity of human cortical neurons.

Limitation of the study

The present results demonstrated the spatiotemporal dynamics of the transcription factors and the histone-modifying enzymes by carefully analyzing the nuclear locations of these molecules and delineated the specific localization of CREB and its co-localization with RNAPII, BRD4, and activity-dependent transcripts. Yet, this does not mean that these molecules bind and/or interact directly with each other. However, our present findings strongly suggest that these molecules are assembled in a spatiotemporal manner. This approach would give an insight into the molecular mechanisms that have not been elucidated by conventional biochemical and molecular biological studies.

The present study did not directly visualize any CRE sites in the nucleus, but the results in the mutant CREB and cell-free conditions strongly suggest that CREB binds to CRE sites in the genome of human cortical cells (Figures S2G and S2H). The fact that RNAPII accumulation and activity-dependent gene transcription occurred at CREB hotspots further supports this view.

We utilized human ESC-derived cortical neurons to investigate the dynamics of transcription factors and chromatin modifiers. One problem is that cell sampling is biased toward deep-layer neurons rather than upper-layer neurons. Indeed, most cells in the culture condition were CTIP2- or TBR1-positive neurons. Furthermore, these cells may not yet be fully differentiated. It is likely that the extent of neuronal maturation affected activity-dependent responsiveness. As described above, roughly 14% cells did not express phosphorylated CREB in KCl treatment, indicating that these cells were unable to respond to neuronal activity (Figure 1A). The fact that a small population of cells did show neither hotspots nor co-localization of CREB with CBP even with neuronal stimulation may be due to the inactive state of CREB (Figures 2F, 6C, and S3D). Therefore, more plastic aspects in cortical neurons may be obtained by combining an organoid technique, which could lead to important findings to reveal gene regulation mechanisms of cortical plasticity and neuronal diseases.

STAR★METHODS

Detailed methods are provided in the online version of this paper and include the following:

- KEY RESOURCES TABLE
- RESOURCE AVAILABILITY
  - Lead contact
  - Materials availability
  - Data and code availability
- EXPERIMENTAL MODEL AND STUDY PARTICIPANT DETAILS

SUPPLEMENTAL INFORMATION

Supplemental information can be found online at https://doi.org/10.1016/j.celrep.2023.113576.

ACKNOWLEDGMENTS

We thank Drs. Wenbiao Gan and Takeshi Yagi for critical reading and continuous encouragement. We also thank Drs. Akihiko Ishijima and Tetsuro Hirose for useful suggestions. This work was supported by MEXT KAKENHI on "Dynamic regulation of brain function by Scrap & Build system" (no. 16H06460), JSPS KAKENHI grants (nos. 19H03325 to N.Y. and 17K071090 to N.S.), and JST SPRING (no. JPMJSP2138 to Y.A.), and was also supported by the European Research Council (NEUROTEMPO), the Belgian FWO, and FRS/FNRS, the Belgian Queen Elizabeth Foundation to P.V.

AUTHOR CONTRIBUTIONS

A.Y., N.S., and N.Y. designed the studies and conducted the experiments. A.Y., N.S., and N.Y. analyzed data. R.I. and P.V. generated ESC-derived cortical neurons. H.K. generated the RNAPII probe. R.I., P.V., and H.K. were also involved in the data analyses. A.Y., N.S., and N.Y. wrote the manuscript.

DECLARATION OF INTERESTS

The authors declare no competing interests.

INCLUSION AND DIVERSITY

We support inclusive, diverse, and equitable conduct of research.

Received: May 23, 2023
Revised: November 10, 2023
Accepted: November 27, 2023
Published: December 20, 2023

REFERENCES

1. West, A.E., and Greenberg, M.E. (2011). Neuronal activity-regulated gene transcription in synapse development and cognitive function. Cold Spring Harb. Perspect. Biol. *3*, a005744.
2. Yamamoto, N., and López-Bendito, G. (2012). Shaping brain connections through spontaneous neural activity. Eur. J. Neurosci. *35*, 1595–1604.
3. Thompson, A., Gribizis, A., Chen, C., and Crair, M.C. (2017). Activity-dependent development of visual receptive fields. Curr. Opin. Neurobiol. *42*, 136–143.
4. Pumo, G.M., Kitazawa, T., and Rijli, F.M. (2022). Epigenetic and Transcriptional Regulation of Spontaneous and Sensory Activity Dependent Programs During Neuronal Circuit Development. Front. Neural Circuits *16*, 911023.
5. Amir, R.E., Van den Veyver, I.B., Wan, M., Tran, C.Q., Francke, U., and Zoghbi, H.Y. (1999). Rett syndrome is caused by mutations in X-linked MECP2, encoding methyl-CpG-binding protein 2. Nat. Genet. *23*, 185–188.
6. Ebert, D.H., and Greenberg, M.E. (2013). Activity-dependent neuronal signalling and autism spectrum disorder. Nature *493*, 327–337.
7. Boulting, G.L., Durresi, E., Ataman, B., Sherman, M.A., Mei, K., Harmin, D.A., Carter, A.C., Hochbaum, D.R., Granger, A.J., Engreitz, J.M., et al. (2021). Activity-dependent regulome of human GABAergic neurons reveals new patterns of gene regulation and neurological disease heritability. Nat. Neurosci. *24*, 437–448.
8. Impey, S., Fong, A.L., Wang, Y., Cardinaux, J.R., Fass, D.M., Obrietan, K., Wayman, G.A., Storm, D.R., Soderling, T.R., and Goodman, R.H. (2002). Phosphorylation of CBP mediates transcriptional activation by neural activity and CaM kinase IV. Neuron *34*, 235–244.
9. Tyssowski, K.M., DeStefino, N.R., Cho, J.H., Dunn, C.J., Poston, R.G., Carty, C.E., Jones, R.D., Chang, S.M., Romeo, P., Wurzelmann, M.K., et al. (2018). Different Neuronal Activity Patterns Induce Different Gene Expression Programs. Neuron *98*, 530–546.e11.
10. Miyasaka, Y., and Yamamoto, N. (2021). Neuronal Activity Patterns Regulate Brain-Derived Neurotrophic Factor Expression in Cortical Cells via Neuronal Circuits. Front. Neurosci. *15*, 699583.
11. Hardingham, G.E., Arnold, F.J., and Bading, H. (2001). Nuclear calcium signaling controls CREB-mediated gene expression triggered by synaptic activity. Nat. Neurosci. *4*, 261–267.
12. Greer, P.L., and Greenberg, M.E. (2008). From synapse to nucleus: calcium-dependent gene transcription in the control of synapse development and function. Neuron *59*, 846–860.
13. Fowler, T., Sen, R., and Roy, A.L. (2011). Regulation of primary response genes. Mol. Cell *44*, 348–360.
14. Joo, J.Y., Schaukowitch, K., Farbiak, L., Kilaru, G., and Kim, T.K. (2016). Stimulus-specific combinatorial functionality of neuronal c-fos enhancers. Nat. Neurosci. *19*, 75–83.
15. Bito, H., Deisseroth, K., and Tsien, R.W. (1996). CREB phosphorylation and dephosphorylation: a Ca(2+)- and stimulus duration-dependent switch for hippocampal gene expression. Cell *87*, 1203–1214.
16. Mayr, B., and Montminy, M. (2001). Transcriptional regulation by the phosphorylation-dependent factor CREB. Nat. Rev. Mol. Cell Biol. *2*, 599–609.
17. Kornhauser, J.M., Cowan, C.W., Shaywitz, A.J., Dolmetsch, R.E., Griffith, E.C., Hu, L.S., Haddad, C., Xia, Z., and Greenberg, M.E. (2002). CREB transcriptional activity in neurons is regulated by multiple, calcium-specific phosphorylation events. Neuron *34*, 221–233.
18. Lonze, B.E., and Ginty, D.D. (2002). Function and regulation of CREB family transcription factors in the nervous system. Neuron *35*, 605–623.
19. Zhang, X., Odom, D.T., Koo, S.H., Conkright, M.D., Canettieri, G., Best, J., Chen, H., Jenner, R., Herbolsheimer, E., Jacobsen, E., et al. (2005). Genome-wide analysis of cAMP-response element binding protein occupancy, phosphorylation, and target gene activation in human tissues. Proc. Natl. Acad. Sci. USA *102*, 4459–4464.
20. Kim, T.K., Hemberg, M., Gray, J.M., Costa, A.M., Bear, D.M., Wu, J., Harmin, D.A., Laptewicz, M., Barbara-Haley, K., Kuersten, S., et al. (2010). Widespread transcription at neuronal activity-regulated enhancers. Nature *465*, 182–187.

21. Malik, A.N., Vierbuchen, T., Hemberg, M., Rubin, A.A., Ling, E., Couch, C.H., Stroud, H., Spiegel, I., Farh, K.K.H., Harmin, D.A., and Greenberg, M.E. (2014). Genome-wide identification and characterization of functional neuronal activity-dependent enhancers. Nat. Neurosci. *17*, 1330–1339.

22. Chrivia, J.C., Kwok, R.P., Lamb, N., Hagiwara, M., Montminy, M.R., and Goodman, R.H. (1993). Phosphorylated CREB binds specifically to the nuclear protein CBP. Nature *365*, 855–859.

23. Bannister, A.J., and Kouzarides, T. (1996). The CBP co-activator is a histone acetyltransferase. Nature *384*, 641–643.

24. Chen, L.F., Lin, Y.T., Gallegos, D.A., Hazlett, M.F., Gómez-Schiavon, M., Yang, M.G., Kalmeta, B., Zhou, A.S., Holtzman, L., Gersbach, C.A., et al. (2019). Enhancer Histone Acetylation Modulates Transcriptional Bursting Dynamics of Neuronal Activity-Inducible Genes. Cell Rep. *26*, 1174–1188.e5.

25. Esvald, E.E., Tuvikene, J., Sirp, A., Patil, S., Bramham, C.R., and Timmusk, T. (2020). CREB Family Transcription Factors Are Major Mediators of BDNF Transcriptional Autoregulation in Cortical Neurons. J. Neurosci. *40*, 1405–1426.

26. Speil, J., Baumgart, E., Siebrasse, J.P., Veith, R., Vinkemeier, U., and Kubitscheck, U. (2011). Activated STAT1 transcription factors conduct distinct saltatory movements in the cell nucleus. Biophys. J. *101*, 2592–2600.

27. Chen, J., Zhang, Z., Li, L., Chen, B.C., Revyakin, A., Hajj, B., Legant, W., Dahan, M., Lionnet, T., Betzig, E., et al. (2014). Single-molecule dynamics of enhanceosome assembly in embryonic stem cells. Cell *156*, 1274–1285.

28. Liu, Z., Legant, W.R., Chen, B.C., Li, L., Grimm, J.B., Lavis, L.D., Betzig, E., and Tjian, R. (2014). 3D imaging of Sox2 enhancer clusters in embryonic stem cells. Elife *3*, e04236.

29. Hipp, L., Beer, J., Kuchler, O., Reisser, M., Sinske, D., Michaelis, J., Gebhardt, J.C.M., and Knöll, B. (2019). Single-molecule imaging of the transcription factor SRF reveals prolonged chromatin-binding kinetics upon cell stimulation. Proc. Natl. Acad. Sci. USA *116*, 880–889.

30. Sugo, N., Morimatsu, M., Arai, Y., Kousoku, Y., Ohkuni, A., Nomura, T., Yanagida, T., and Yamamoto, N. (2015). Single-Molecule Imaging Reveals Dynamics of CREB Transcription Factor Bound to Its Target Sequence. Sci. Rep. *5*, 10662.

31. Kitagawa, H., Sugo, N., Morimatsu, M., Arai, Y., Yanagida, T., and Yamamoto, N. (2017). Activity-Dependent Dynamics of the Transcription Factor of cAMP-Response Element Binding Protein in Cortical Neurons Revealed by Single-Molecule Imaging. J. Neurosci. *37*, 1–10.

32. Uchino, S., Ito, Y., Sato, Y., Handa, T., Ohkawa, Y., Tokunaga, M., and Kimura, H. (2022). Live imaging of transcription sites using an elongating RNA polymerase II-specific probe. J. Cell Biol. *221*, e202104134.

33. Ohishi, H., Shimada, S., Uchino, S., Li, J., Sato, Y., Shintani, M., Owada, H., Ohkawa, Y., Pertsinidis, A., Yamamoto, T., et al. (2022). STREAMING-tag system reveals spatiotemporal relationships between transcriptional regulatory factors and transcriptional activity. Nat. Commun. *13*, 7672.

34. Specht, C.G., Izeddin, I., Rodriguez, P.C., El Beheiry, M., Rostaing, P., Darzacq, X., Dahan, M., and Triller, A. (2013). Quantitative nanoscopy of inhibitory synapses: counting gephyrin molecules and receptor binding sites. Neuron *79*, 308–321.

35. Zhan, H., Stanciauskas, R., Stigloher, C., Keomanee-Dizon, K., Jospin, M., Bessereau, J.L., and Pinaud, F. (2014). In vivo single-molecule imaging identifies altered dynamics of calcium channels in dystrophin-mutant C. elegans. Nat. Commun. *5*, 4974.

36. Renner, M., Wang, L., Levi, S., Hennekinne, L., and Triller, A. (2017). A Simple and Powerful Analysis of Lateral Subdiffusion Using Single Particle Tracking. Biophys. J. *113*, 2452–2463.

37. Nozaki, T., Imai, R., Tanbo, M., Nagashima, R., Tamura, S., Tani, T., Joti, Y., Tomita, M., Hibino, K., Kanemaki, M.T., et al. (2017). Dynamic Organization of Chromatin Domains Revealed by Super-Resolution Live-Cell Imaging. Mol. Cell *67*, 282–293.e7.

38. Kaplan, L., Ierokomos, A., Chowdary, P., Bryant, Z., and Cui, B. (2018). Rotation of endosomes demonstrates coordination of molecular motors during axonal transport. Sci. Adv. *4*, e1602170.

39. Yamamoto, N., and Okada, Y. (2020). Single Molecule Microscopy in Neurobiology (Springer).

40. Petrij, F., Giles, R.H., Dauwerse, H.G., Saris, J.J., Hennekam, R.C., Masuno, M., Tommerup, N., van Ommen, G.J., Goodman, R.H., Peters, D.J., et al. (1995). Rubinstein-Taybi syndrome caused by mutations in the transcriptional co-activator CBP. Nature *376*, 348–351.

41. Spena, S., Milani, D., Rusconi, D., Negri, G., Colapietro, P., Elcioglu, N., Bedeschi, F., Pilotta, A., Spaccini, L., Ficcadenti, A., et al. (2015). Insights into genotype-phenotype correlations from CREBBP point mutation screening in a cohort of 46 Rubinstein-Taybi syndrome patients. Clin. Genet. *88*, 431–440.

42. Korzus, E. (2017). Rubinstein-Taybi Syndrome and Epigenetic Alterations. Adv. Exp. Med. Biol. *978*, 39–62.

43. Espuny-Camacho, I., Michelsen, K.A., Gall, D., Linaro, D., Hasche, A., Bonnefont, J., Bali, C., Orduz, D., Bilheu, A., Herpoel, A., et al. (2013). Pyramidal neurons derived from human pluripotent stem cells integrate efficiently into mouse brain circuits in vivo. Neuron *77*, 440–456.

44. Shi, Y., Kirwan, P., Smith, J., Robinson, H.P.C., and Livesey, F.J. (2012). Human cerebral cortex development from pluripotent stem cells to functional excitatory synapses. Nat. Neurosci. *15*, 477–486.

45. Linaro, D., Vermaercke, B., Iwata, R., Ramaswamy, A., Libé-Philippot, B., Boubakar, L., Davis, B.A., Wierda, K., Davie, K., Poovathingal, S., et al. (2019). Xenotransplanted Human Cortical Neurons Reveal Species-Specific Development and Functional Integration into Mouse Visual Circuits. Neuron *104*, 972–986.e6.

46. Bading, H., Ginty, D.D., and Greenberg, M.E. (1993). Regulation of gene expression in hippocampal neurons by distinct calcium signaling pathways. Science *260*, 181–186.

47. Tokunaga, M., Imamoto, N., and Sakata-Sogawa, K. (2008). Highly inclined thin illumination enables clear single-molecule imaging in cells. Nat. Methods *5*, 159–161.

48. Walton, K.M., Rehfuss, R.P., Chrivia, J.C., Lochner, J.E., and Goodman, R.H. (1992). A dominant repressor of cyclic adenosine 3',5'-monophosphate (cAMP)-regulated enhancer-binding protein activity inhibits the cAMP-mediated induction of the somatostatin promoter in vivo. Mol. Endocrinol. *6*, 647–655.

49. Cook, P.R. (1999). The organization of replication and transcription. Science *284*, 1790–1795.

50. Yao, J., Ardehali, M.B., Fecko, C.J., Webb, W.W., and Lis, J.T. (2007). Intranuclear distribution and local dynamics of RNA polymerase II during transcription activation. Mol. Cell *28*, 978–990.

51. Li, J., Dong, A., Saydaminova, K., Chang, H., Wang, G., Ochiai, H., Yamamoto, T., and Pertsinidis, A. (2019). Single-Molecule Nanoscopy Elucidates RNA Polymerase II Transcription at Single Genes in Live Cells. Cell *178*, 491–506.e28.

52. Buratowski, S. (2009). Progression through the RNA polymerase II CTD cycle. Mol. Cell *36*, 541–546.

53. Marmorstein, R., and Zhou, M.M. (2014). Writers and readers of histone acetylation: structure, mechanism, and inhibition. Cold Spring Harb. Perspect. Biol. *6*, a018762.

54. Filippakopoulos, P., Picaud, S., Mangos, M., Keates, T., Lambert, J.P., Barsyte-Lovejoy, D., Felletar, I., Volkmer, R., Müller, S., Pawson, T., et al. (2012). Histone recognition and large-scale structural analysis of the human bromodomain family. Cell *149*, 214–231.

55. Lovén, J., Hoke, H.A., Lin, C.Y., Lau, A., Orlando, D.A., Vakoc, C.R., Bradner, J.E., Lee, T.I., and Young, R.A. (2013). Selective inhibition of tumor oncogenes by disruption of super-enhancers. Cell *153*, 320–334.

56. Korzus, E., Rosenfeld, M.G., and Mayford, M. (2004). CBP histone acetyltransferase activity is a critical component of memory consolidation. Neuron *42*, 961–972.

57. Niewidok, B., Igaev, M., Pereira da Graca, A., Strassner, A., Lenzen, C., Richter, C.P., Piehler, J., Kurre, R., and Brandt, R. (2018). Single-molecule imaging reveals dynamic biphasic partition of RNA-binding proteins in stress granules. J. Cell Biol. *217*, 1303–1318.

58. Joensuu, M., Martínez-Mármol, R., Padmanabhan, P., Glass, N.R., Durisic, N., Pelekanos, M., Mollazade, M., Balistreri, G., Amor, R., Cooper-White, J.J., et al. (2017). Visualizing endocytic recycling and trafficking in live neurons by subdiffractional tracking of internalized molecules. Nat. Protoc. *12*, 2590–2622.

59. Kuchler, O., Gerlach, J., Vomhof, T., Hettich, J., Steinmetz, J., Gebhardt, J.C.M., Michaelis, J., and Knöll, B. (2022). Single-molecule tracking (SMT) and localization of SRF and MRTF transcription factors during neuronal stimulation and differentiation. Open Biol. *12*, 210383.

60. Presman, D.M., Ball, D.A., Paakinaho, V., Grimm, J.B., Lavis, L.D., Karpova, T.S., and Hager, G.L. (2017). Quantifying transcription factor binding dynamics at the single-molecule level in live cells. Methods *123*, 76–88. https://doi.org/10.1016/j.ymeth.2017.03.014.

61. Du, K., Asahara, H., Jhala, U.S., Wagner, B.L., and Montminy, M. (2000). Characterization of a CREB gain-of-function mutant with constitutive transcriptional activity in vivo. Mol. Cell Biol. *20*, 4320–4327.

62. Suzuki, A., Fukushima, H., Mukawa, T., Toyoda, H., Wu, L.J., Zhao, M.G., Xu, H., Shang, Y., Endoh, K., Iwamoto, T., et al. (2011). Upregulation of CREB-mediated transcription enhances both short- and long-term memory. J. Neurosci. *31*, 8786–8802.

63. McNally, J.G., Müller, W.G., Walker, D., Wolford, R., and Hager, G.L. (2000). The glucocorticoid receptor: rapid exchange with regulatory sites in living cells. Science *287*, 1262–1265.

64. Rayasam, G.V., Elbi, C., Walker, D.A., Wolford, R., Fletcher, T.M., Edwards, D.P., and Hager, G.L. (2005). Ligand-specific dynamics of the progesterone receptor in living cells and during chromatin remodeling in vitro. Mol. Cell Biol. *25*, 2406–2418.

65. Sharp, Z.D., Mancini, M.G., Hinojos, C.A., Dai, F., Berno, V., Szafran, A.T., Smith, K.P., Lele, T.P., Ingber, D.E., and Mancini, M.A. (2006). Estrogen-receptor-alpha exchange and chromatin dynamics are ligand- and domain-dependent. J. Cell Sci. *119*, 4101–4116.

66. Sabari, B.R., Dall'Agnese, A., Boija, A., Klein, I.A., Coffey, E.L., Shrinivas, K., Abraham, B.J., Hannett, N.M., Zamudio, A.V., Manteiga, J.C., et al. (2018). Coactivator condensation at super-enhancers links phase separation and gene control. Science *361*, eaar3958.

67. Kim, S.K., Liu, X., Park, J., Um, D., Kilaru, G., Chiang, C.M., Kang, M., Huber, K.M., Kang, K., and Kim, T.K. (2021). Functional coordination of BET family proteins underlies altered transcription associated with memory impairment in fragile X syndrome. Sci. Adv. *7*, eabf7346.

68. Linseman, D.A., Bartley, C.M., Le, S.S., Laessig, T.A., Bouchard, R.J., Meintzer, M.K., Li, M., and Heidenreich, K.A. (2003). Inactivation of the myocyte enhancer factor-2 repressor histone deacetylase-5 by endogenous Ca(2+)//calmodulin-dependent kinase II promotes depolarization-mediated cerebellar granule neuron survival. J. Biol. Chem. *278*, 41472–41481.

69. Sugo, N., Oshiro, H., Takemura, M., Kobayashi, T., Kohno, Y., Uesaka, N., Song, W.J., and Yamamoto, N. (2010). Nucleocytoplasmic translocation of HDAC9 regulates gene expression and dendritic growth in developing cortical neurons. Eur. J. Neurosci. *31*, 1521–1532.

70. Narita, T., Ito, S., Higashijima, Y., Chu, W.K., Neumann, K., Walter, J., Satpathy, S., Liebner, T., Hamilton, W.B., Maskey, E., et al. (2021). Enhancers are activated by p300/CBP activity-dependent PIC assembly, RNAPII recruitment, and pause release. Mol. Cell *81*, 2166–2182.e6.

71. Alari, V., Russo, S., Terragni, B., Ajmone, P.F., Sironi, A., Catusi, I., Calzari, L., Concolino, D., Marotta, R., Milani, D., et al. (2018). iPSC-derived neurons of CREBBP- and EP300-mutated Rubinstein-Taybi syndrome patients show morphological alterations and hypoexcitability. Stem Cell Res. *30*, 130–140.

72. Alari, V., Scalmani, P., Ajmone, P.F., Perego, S., Avignone, S., Catusi, I., Lonati, P.A., Borghi, M.O., Finelli, P., Terragni, B., et al. (2021). Histone Deacetylase Inhibitors Ameliorate Morphological Defects and Hypoexcitability of iPSC-Neurons from Rubinstein-Taybi Patients. Int. J. Mol. Sci. *22*, 5777.

73. Wood, M.A., Kaplan, M.P., Park, A., Blanchard, E.J., Oliveira, A.M.M., Lombardi, T.L., and Abel, T. (2005). Transgenic mice expressing a truncated form of CREB-binding protein (CBP) exhibit deficits in hippocampal synaptic plasticity and memory storage. Learn. Mem. *12*, 111–119.

74. Vieira, P.A., and Korzus, E. (2015). CBP-Dependent memory consolidation in the prefrontal cortex supports object-location learning. Hippocampus *25*, 1532–1540.

75. Girskis, K.M., Stergachis, A.B., DeGennaro, E.M., Doan, R.N., Qian, X., Johnson, M.B., Wang, P.P., Sejourne, G.M., Nagy, M.A., Pollina, E.A., et al. (2021). Rewiring of human neurodevelopmental gene regulatory programs by human accelerated regions. Neuron *109*, 3239–3251.e7.

76. Shulha, H.P., Crisci, J.L., Reshetov, D., Tushir, J.S., Cheung, I., Bharadwaj, R., Chou, H.J., Houston, I.B., Peter, C.J., Mitchell, A.C., et al. (2012). Human-specific histone methylation signatures at transcription start sites in prefrontal neurons. PLoS Biol. *10*, e1001427.

77. Stewart-Ornstein, J., Cheng, H.W.J., and Lahav, G. (2017). Conservation and Divergence of p53 Oscillation Dynamics across Species. Cell Syst. *5*, 410–417.e4.

78. Matsuda, M., Hayashi, H., Garcia-Ojalvo, J., Yoshioka-Kobayashi, K., Kageyama, R., Yamanaka, Y., Ikeya, M., Toguchida, J., Alev, C., and Ebisuya, M. (2020). Species-specific segmentation clock periods are due to differential biochemical reaction speeds. Science *369*, 1450–1455.

79. Iwata, R., Casimir, P., Erkol, E., Boubakar, L., Planque, M., Gallego López, I.M., Ditkowska, M., Gaspariunaite, V., Beckers, S., Remans, D., et al. (2023). Mitochondria metabolism sets the species-specific tempo of neuronal development. Science *379*, eabn4705.

80. Hatanaka, Y., and Murakami, F. (2002). In vitro analysis of the origin, migratory behavior, and maturation of cortical pyramidal cells. J. Comp. Neurol. *454*, 1–14.

81. Malyshevskaya, O., Shiraishi, Y., Kimura, F., and Yamamoto, N. (2013). Role of electrical activity in horizontal axon growth in the developing cortex: a time-lapse study using optogenetic stimulation. PLoS One *8*, e82954.

82. Gong, F., Chiu, L.Y., Cox, B., Aymard, F., Clouaire, T., Leung, J.W., Cammarata, M., Perez, M., Agarwal, P., Brodbelt, J.S., et al. (2015). Screen identifies bromodomain protein ZMYND8 in chromatin recognition of transcription-associated DNA damage that promotes homologous recombination. Genes Dev. *29*, 197–211.

Please cite this article in press as: Atsumi et al., Repetitive CREB-DNA interactions at gene loci predetermined by CBP induce activity-dependent gene expression in human cortical neurons, Cell Reports (2023), https://doi.org/10.1016/j.celrep.2023.113576

STAR★METHODS

KEY RESOURCES TABLE

REAGENT or RESOURCE	SOURCE	IDENTIFIER
Antibodies		
Anti-TBR1, Rabbit Polyclonal	Abcam	Cat#: ab31940; RRID: AB_2200219
Anti-CTIP2, Rat Monoclonal	Abcam	Cat#: ab18465; RRID: AB_2064130
Anti-MAP2, Mouse Monoclonal	Sigma	Cat#: M1406; RRID: AB_477171
Anti-BRN2, Goat Polyclonal	Santa Cruz	Cat#: sc-6029; RRID: AB_2167385
Anti-GFAP, Rabbit Polyclonal	Sigma	Cat#: G9269; RRID: AB_477035
Anti-VGLUT1, Rabbit Polyclonal	Synaptic Systems	Cat#: 135303; RRID: AB_887875
Anti-PSD95, Mouse Monoclonal	Abcam	Cat#: ab2723; RRID: AB_303248
Anti-CREB, Mouse Monoclonal	Cell Signaling Technology	Cat#: 9104; RRID: AB_490881
Anti-Phosphorylated CREB (Ser133), Rabbit Monoclonal	Cell Signaling Technology	Cat#: 9198; RRID: AB_2561044
Anti-FOS, Rabbit Polyclonal	Abcam	Cat#: ab190289; RRID: AB_2737414
Anti-BRD4, Rabbit Monoclonal	Abcam	Cat#: ab128874; RRID: AB_11145462
Anti-acetyl-Histone H4, Rabbit Polyclonal	Sigma	Cat#: 06–866; RRID: AB_310270
Anti-Rabbit IgG Alexa Flour 488, Goat Polyclonal	Thermo Fisher	Cat#: A11034; RRID: AB_2576217
Anti-Goat IgG Alexa Flour 488, Donkey Polyclonal	Abcam	Cat#: ab150129; RRID: AB_2687506
Anti-Rat IgG Cy3, Goat Polyclonal	Millipore	Cat#: AP183C; RRID: AB_92596
Anti-Mouse IgG Cy3, Donkey Polyclonal	Millipore	Cat#: AP192C; RRID: AB_92642
Anti-Mouse IgG Alexa Flour 594, Donkey Polyclonal	Thermo Fisher	Cat#: A21203; RRID: AB_141633
Anti-Mouse IgG Cy5, Goat Polyclonal	Jackson ImmunoResearch	Cat#: 115-175-166; RRID: AB_2338714
Chemicals, peptides, and recombinant proteins		
Poly-L-ornithine	Sigma	Cat#: P3655
Matrigel	Corning	Cat#: 356234
DMEM/F-12	Gibco	Cat#: 11320-033
Doxycycline	Clontech	Cat#:631311
TMR direct-conjugated HaloTag ligand	Promega	Cat#: G2991
TMR-conjugated HaloTag ligand	Promega	Cat#: G8251
SaraFluor 650T-conjugated HaloTag ligand	Goryo Chemical	Cat#: A308-01
647SiR-conjugated SNAPtag ligand	NEB	Cat#: S9102S
Formaldehyde	Sigma	Cat#: F8775
Normal donkey serum	Jackson ImmunoResearch	Cat#: 017-000-121
Normal goat serum	Vector laboratory	Cat#: S-1000
DAPI	Sigma	Cat#: D9542
Antifade Mounting Medium	Vector Laboratories	Cat#: H-1000
Critical commercial assays		
Maxiprep Kit	Qiagen	Cat#: 12163 or 12362
TNT Quick Coupled Transcription/Translation System	Promega	Cat#: L1170
Experimental models: Cell lines		
Human: H9 ES cells	Espuny-Camacho et al.[43]	N/A
Oligonucleotides		
human *FOS* intron with Quasar 570	LGC Biosearch	N/A

(*Continued on next page*)

Please cite this article in press as: Atsumi et al., Repetitive CREB-DNA interactions at gene loci predetermined by CBP induce activity-dependent gene expression in human cortical neurons, Cell Reports (2023), https://doi.org/10.1016/j.celrep.2023.113576

Continued

REAGENT or RESOURCE	SOURCE	IDENTIFIER
human NR4A1 intron with Quasar 670	LGC Biosearch	N/A
human GAPDH intron with Quasar 670	LGC Biosearch	N/A
Recombinant DNA		
Plasmid: pTet-On Advance/TRE-Tight HaloTag-human CREB	Kitagawa et al.[31]	N/A
Plasmid: pTα1-EGFP	Hatanaka et al.[80]	N/A
Plasmid: pTα1-Dsred2	Hatanaka et al.[80]	N/A
Plasmid: pCMV-HaloTag-human CREB	Promega	Clone name: pFN21AB5414
Plasmid: pCAGGS-hChR2(H134R)-EYFP	Malyshevskaya et al.[81]	N/A
Plasmid: pB533-44B12mut23-sfGFP	Ohishi et al.[33]	Addgene plasmid #186778
Plasmid: pCMV-GFP-BRD4	Gong et al.[82]	Addgene plasmid #65378
Plasmid: pCAGGS-EGFP-CBP	This paper	N/A
Plasmid: pCAGGS-EGFP-CBP (Y1540A/F1541A)	This paper	N/A
Plasmid: pTRE-SNAPtag-CBP	This paper	N/A
Plasmid: pTRE-SNAPtag alone	This paper	N/A
Plasmid: pTet-On Advance/TRE-Tight HaloTag-human CREB (Y134F)	This paper	N/A
Software and algorithms		
ImageJ	NIH, USA	http://fiji.sc; RRID:SCR_002285
Origin 2021 software	OriginLab	http://www.originlab.com/index.aspx?go=PRODUCTS/Origin; RRID:SCR_014212
R (x64 version 3.5.1)	R Foundation for Statistical Computing	http://www.r-project.org/; SCR_001905
Other		
35 mm glass bottomed dishes	Greiner Bio-One	Cat#: 627860
CUY21EX Electroporator	BEX	N/A

RESOURCE AVAILABILITY

Lead contact

Further information and requests for resources and reagents should be directed to and will be fulfilled by the lead contact, Noriyuki Sugo (sugo@fbs.osaka-u.ac.jp).

Materials availability

All materials generated in this study will be available upon request with a completed Materials Transfer Agreement.

Data and code availability

- All data reported in this paper will be shared by the lead contact upon request.
- This paper does not report original code.
- Any additional information required to reanalyze the data reported in this paper is available from the lead contact upon request.

EXPERIMENTAL MODEL AND STUDY PARTICIPANT DETAILS

Human ESC differentiation into cortical cells

All experiments using human ESCs and neural stem cells were conducted with the approval of the VIB, KU Leuven and Osaka University Ethical Committees. To generate human cortical cells, H9 ESCs were plated with human ES medium containing 10 μM ROCK-inhibitor Y27632.[43] Two days later (0 DIV), the medium was exchanged to the culture medium containing 100 ng/mL Noggin for 25 days. The obtained neural stem cells were further expanded for about a week and frozen in vials in liquid nitrogen. These frozen cells were used as neuroepithelial and radial glial cells for cortical cell differentiation. One day before plating, glass bottomed dishes (Greiner Bio-One, 627860) were coated by 0.1 mg/mL Poly-L-ornithine (Sigma, P3655) for longer than 3 h and subsequently by

Matrigel (Corning, 356234) only in the center of dishes (5 mm diameter) for at least 2 h. After thawing, 1–2 x 10^4 cells were plated at the Matrigel-coated area with the culture medium. The medium was replaced every one week.

METHOD DETAILS

Plasmids

To study CREB dynamics at the single-molecule level, a Tet-inducible HaloTag-CREB expression vector, pTet-On Advance/TRE-Tight HaloTag-human CREB, was used.[31] To label neurons, α tubulin promoter-driven EGFP (pTα1-EGFP) or dsRed2 (pTα1-Dsred) expression vectors was used.[80] To perform optogenetic stimulation, pCAGGS-hChR2(H134R)-EYFP was used. To visualize accumulation of RNAPII, pB533-44B12mut23-sfGFP encoding GFP-tagged Ser5ph RNAPII-specific probe was used.[33] Commercially available pCMV-GFP-BRD4 (addgene, 65378) was used to examine BRD4 distribution in live imaging.[82] To generate pCAGGS-EGFP-CBP expression vector, human CBP cDNA (Promega, pFN24K) was inserted into AsisI and PmeI sites in pCAGGS-EGFP. To make a CBP mutation in HAT domain (Y1540A/F1541A),[56] pCAGGS-EGFP-CBP was amplified by PCR with the mutagenesis primer pairs: 5′-TGGGCCAGAAATCACCTTCAGCAGCGGGCAGTTCCTTGGCACTGG-3′ and 5′- CCAGTGCCAAGGAACTGCCC GCTGCTGAAGGTGATTTCTGGCCCA -3’. The PCR product and pCAGGS-EGFP-CBP were digested by AsisI and PmeI, and human CBP mutant (dHAT) was inserted. To generate pTRE-SNAPtag-CBP, pTRE-tight SNAPtag-TORC1 was digested by AsisI and PmeI sites, and human CBP cDNA was inserted. To generate pTRE-SNAPtag alone, human CBP was digested by AsisI and PmeI sites. To generate pTet-On Advance/TRE-Tight HaloTag-human CREB (Y134F), a CREB mutation was performed. The PCR product and pTet-On Advance/TRE-Tight HaloTag-human CREB was digested by AsisI and PmeI, and human CREB mutant (Y134F) was inserted. All plasmids were harvested using Maxiprep Kit (Qiagen, 12163 or 12362).

Pharmacological experiment

To stimulate cultured cells, 0.41 volumes of KCl depolarization solution (170 mM KCl, 1.3 mM $MgCl_2$, 0.9 mM $CaCl_2$, 10 mM HEPES, pH 7.4) was added to the culture medium 1 h before the SMI.[31] To examine the expression levels of FOS, BRD4 and H4ac using immunocytochemistry, the depolarization solution was added 3 h before fixation.

In vitro electroporation

Transfection of the plasmids into cultured neurons was performed with an electroporation technique.[31] In brief, 0.1–0.5 μg/μL plasmid solution in 0.2 mL PBS was added to cultured cells on the glass bottomed dishes, and electric pulses composed of one 275 V pulse of 7 ms duration and five 20 V pulses of 50 ms duration were applied at 50 ms intervals through plate electrodes (CUY21EX, BEX). The cultures were washed with PBS and immersed in the original culture medium.

SMI

For the expression of HaloTag-CREB, cells were electroporated with pTet-On Advance/TRE-Tight HaloTag-human CREB (wild type, R301L or Y134F).[30,31,39] One day before observation, 10–50 ng/mL doxycycline (Clontech, 631311) was added to the medium. To visualize HaloTag-CREB, the cultures were incubated with DMEM/F-12 containing 10 nM TMR direct-conjugated HaloTag ligand (Promega, G2991) or SaraFluor 650T-conjugated HaloTag ligand (Goryo Chemical, A308-01) for 15–30 min at 37°C.

An inverted microscope (Ti-E, Nikon) with an oil-immersion objective lens (x100, numerical aperture 1.49, Nikon) and HILO illumination was used to perform single-molecular imaging. The final magnification was 107 nm/pixel. The glass bottomed dish was mounted on a stage top incubator (Tokai Hit) and maintained at 37°C in a humidified atmosphere (5% CO2/95% air). Either TMR or 650T was visualized by HILO illumination with 561 nm (20 mW, Coherent) or 640 nm (40 mW, Coherent) lasers, respectively. Images were obtained at 10 frames per second for 2 min using an EM-CCD (iXon897, Andor Technology) with Solis software (Andor Technology).

To perform simultaneous imaging of HaloTag-CREB and SNAPtag-CBP or SNAPtag alone, cells were electroporated with pTet-On Advance/TRE-Tight HaloTag-CREB and pTRE-SNAPtag-CBP or pTRE-SNAPtag alone. After adding doxycycline, the transfected cells were incubated with a mixture of TMR-conjugated HaloTag ligand and 647SiR-conjugated SNAPtag ligand (NEB, S9102S). Both fluorescent dyes were excited by HILO illumination with 561 nm and 640 nm lasers. The images obtained by simultaneous excitation were separated using an image splitting optics W-VIEW GEMINI (Hamamatsu Photonics) with a 640 nm long-pass dichroic mirror (Semrock FF640-FDi01–25 × 36), and were collected using two bypass filters (Semrock FF01-593/40-25 for 593 nm and FF01-692/40-25 for 692 nm). Split images were obtained at 10 frames per second for 1–2 min using the EM-CCD with NIS-Elements software (Nikon). Aberration had been corrected using 0.1 μm TetraSpeck Fluorescent Microspheres (ThermoFisher, T7284).

For simultaneous observation of HaloTag-CREB at the single-molecule level and Ser5ph RNAPII-GFP signals, cells were electroporated with pTet-On Advance/TRE-Tight HaloTag-CREB and pB533-44B12mut23-sfGFP. After adding doxycycline, the transfected cells were incubated with 650T HaloTag ligand, and HILO illumination with 640 nm and 488 nm (20 mW, Coherent) lasers was used for excitation. The obtained images were separated using the image splitting optics and collected via two bypass filters (Edmund Optics 86951 for 525 nm and Semrock FF01-692/40-25 for 692 nm), as described above.

To examine the spatial relationship between BRD4 and CREB, pCMV-GFP-BRD4 was cotransfected with pTet-On Advance/TRE-Tight HaloTag-CREB. Before and after SMI of CREB, GFP signal containing images were collected under epi-fluorescent excitation light (488 nm, Nikon).

Immunocytochemistry

Cultured cells were fixed with 4% paraformaldehyde in PBS at room temperature for 10 min or 1 h. For staining for VGlut1 and PSD95, the cells were fixed with 1% paraformaldehyde at room temperature for 3 min, followed by ice-cold methanol for 15 min. After incubation with PBS containing 0.3% Triton X-100 (PBST) for 30 min, the cells were subjected to primary antibodies in a blocking buffer, composed of 2% normal donkey serum (Jackson ImmunoResearch, 017-000-121) or normal goat serum (Vector laboratory, S-1000) in PBST at 4°C for overnight. After washing, the cells were incubated with secondary antibodies in PBST at room temperature for 2 h. After washing, the cells were mounted by a medium containing 80% glycerol and 2.3% 1,4-diazabicyclo [2.2.2] octane (Sigma-Aldrich, D2522-25G), and 0.1% 4′,6-diamidino-2-phenylimdole (DAPI, Sigma-Aldrich) in 50 mM Tris-HCl. Finally, the cells were observed with a Axioskop 2 plus (Zeiss) or confocal microscopy, DM6000 CS (Leica).

Interactions between CREB and CRE in cell-free conditions using SMI

A flow cell assembled from two cover glasses was prepared.[30] Biotin-labeled dsDNAs (40 nM in PBS) were adsorbed onto the cover glass surface. Biotin-labeled 19-nt dsDNA including the CRE sequence was prepared by annealing 5′-GACAGCGCACGTC AAGGCA-biotin -3′ and its complementary oligonucleotide. Biotin-labeled 22-nt dsDNA including the κB sequence was prepared by annealing 5′-AGTTGAGGGGACTTTCCCAGGC-biotin-3′ and its complementary oligonucleotide. The flow cell was treated with 10 mg/mL BSA in PBS for 5 min and then flushed with a binding buffer solution (100 mM KCl, 1 mM $MgCl_2$, 20 mM HEPES-NaOH (pH 7.8), 0.1 M DTT, 2 mg/mL BSA, 50% sucrose). In experiments, TMR-CREB in binding buffer was loaded into the flow cell. HaloTag CREB proteins were generated by the TNT Quick Coupled Transcription/Translation System (Promega) with plasmids encoding HaloTag-human CREB1 cDNA (Promega) and labeled with HaloTag TMR Ligand (Promega).

Optogenetic stimulation

An optogenetic experiment was performed by applying excitation light to ChR2-transfected cells.[10,31,81] In brief, a solid-state illuminator (475 nm, 20 mW, Lumencor SPECTRA) was used under the control of a stimulator (A.M.P.I, Master-9). The light stimulation (50 ms duration) was applied with 2 Hz for 5 min through a 100× objective lens.

RNA fluorescence *in situ* hybridization coupled with immunocytochemistry

RNA FISH experiments combined with immunocytochemistry were carried out according to manufacturer's instruction (https://biosearchassets.blob.core.windows.net/assets/bti_custom_stellaris_immunofluorescence_protocol.pdf, LGC Biosearch) with a slight modification. Stellaris RNA FISH Probes were customized for human *FOS* intron with Quasar 570, human *NR4A1* intron with Quasar 670 and human *GAPDH* intron with Quasar 670 (LGC Biosearch). Cells on the glass bottom dishes were fixed in 3.7% formaldehyde (SIGMA, F8775-25ML) at room temperature for 10 min, and permeabilized in 70% ethanol at 4°C for overnight. The cells were hybridized with 125 nM of the RNA probes in hybridization buffer at 37°C for 4–16 h, and incubated with first antibodies at 4°C for overnight and with secondary antibodies in PBST at room temperature for 2 h. The cells were mounted with Antifade Mounting Medium (Vector Laboratories, H-1000) containing 5 ng/mL DAPI. Fifty z-stacks with a 0.2 μm step size and 100 ms exposure time were obtained using the EM-CCD, and deconvolved by NIS-Elements software (Nikon).

QUANTIFICATION AND STATISTICAL ANALYSIS

Spatiotemporal analysis of SMI

All fluorescence images were analyzed by ImageJ software with a plugin, Particle Track and Analysis[30,31] and Origin software (OriginLab). To quantify the temporal dynamics of individual CREB spots, the center coordinate of each spot was determined (using x/y) by Gaussian fitting, and the residence time was measured. The cumulative residence time distribution was fitted by the sum of two exponential curves, $F(t) = A_0 + A_1 (1 - \exp(-t/t_1)) + A_2 (1 - \exp(-t/t_2))$ (Equation 1), using the Levenberg-Marquardt chi-square minimization algorithm. A_0 is constant. A_1 and A_2 are the fractions with time constants t_1 and t_2, respectively ($t_1 < t_2$). When the chi-square tolerance value was less than 1×10^{-9}, the fit was deemed appropriate. Similarly, single-molecule CBP spots were tracked and the residence time distribution was fitted by Equation 1.

To determine the time which separates the long and short residence components, the time was calculated such that the ratio of the short residence component, $A_1 \exp(-t/t_1)/(A_0 + A_1 \exp(-t/t_1) + A_2 \exp(-t/t_2))$, is sufficiently small (<3%). As a result, the boundary times for CREB and CBP spots were determined to be 1 s and 0.6 s, respectively.

To quantify the spatial features of CREB dynamics, the micro-domain was determined by the sum of the maximum fluctuation of the estimated center coordinates for long residence CREB spots and the microscopic stage movement over a 2-min live imaging period. The fluctuation ranges (1.96σ for the center coordinates) were determined by fitting the motion of CREB spots into a Gaussian distribution. The maximum value of fluctuation for TMR- or 650T-CREB (3.7 pixel, 0.40 μm, n = 44 spots) was then added to the microscopic stage movement (1.0 ± 0.1 pixel, 0.11 ± 0.01 μm, n = 20 spots), and the sum was defined as one-side of the micro-domain (0.54 × 0.54 μm, 5 × 5 pixel).

To quantify repetitive CREB appearance, the area covering the whole nucleus in a neuron was divided into 1024 (32 × 32) equal micro-domains. The number of long residence CREB spots was counted in each micro-domain, and normalized by the total number of long residence CREB spots. This value was used as frequency. Mean and SD of the frequency were calculated for all micro-domains

under the unstimulated condition. The micro-domains with >mean + 4 SD, which were hardly observed in the unstimulated condition, were defined as a hotspot.

Analysis of RNAPII distribution with single-molecule CREB

As described above, RNAPII-GFP images were obtained simultaneously with SMI of HaloTag-CREB. RNAPII-GFP images were averaged per 32 frames as the signals were rather noisy. $(F-F_0)/F_0$ was referred as the relative intensity of Ser5ph RNAPII-GFP. F is the GFP intensity, and F_0 is the average of F from 0 s to 10 s. To quantify the correlation between CREB spots and RNAPII-GFP signals, the number of long residence CREB spots and the time integral values of RNAPII-GFP for the CREB residence time plus the subsequent 10 s were calculated for each micro-domain. In this analysis, the subnuclear domain for RNAPII-GFP was defined as 10 pixels square (1.07 × 1.07 μm) because the signals were broader than those for CREB spots (see Figure 3A).

Quantification of BRD4 and H4ac signals after immunocytochemistry

Immunostaining images with anti-BRD4 and anti-H4ac were obtained by 50 z-stacks with a 0.2 μm step size. After the background subtraction, the number and the volume of these spots per cell were measured by ImageJ.

Colocalization analyses

As for colocalization of CREB and CBP during simultaneous live imaging, when the distance between the center coordinates of TMR-CREB and 647SiR-CBP is smaller than the sum of fluctuation ranges of CREB (0.10 ± 0.01 μm, n = 22 spots) and those of CBP (0.10 ± 0.01 μm, n = 26 spots), these spots were defined as colocalization (0.20 μm = 0.10 + 0.10). The fluctuation was obtained by fitting the motion into a 2D Gaussian distribution, and a value twice the standard deviation was used as the fluctuation range.

As for colocalization of 650T-CREB and GFP-BRD4 spots, when the distance between the center coordinates of 650T-CREB and GFP-BRD4 spots was smaller than the sum of the fluctuation ranges of CREB spots (0.13 ± 0.01 μm, n = 44 spots), the radius of GFP-BRD4 spots (0.29 ± 0.01 μm, n = 36 spots, the radius was used since GFP-BRD4 spots were not single molecules) and the microscopic stage movement over a 2-min live imaging period (0.11 ± 0.01 μm, n = 20 spots), these spots were defined as colocalization (0.53 μm = 0.13 + 0.29 + 0.11). The spatial distribution of GFP-BRD4 spot intensities was fitted by a 2D Gaussian distribution, and a value twice the standard deviation was used as the radius.

As for colocalization of RNA FISH with immunopositive spots, when the distance between the center coordinates of two spots was smaller than the sum of the radii of these two spots, these two spots were defined as colocalization. The radius of each spot was determined similarly to BRD4-GFP as these spots also did not represent single molecules. The radii were 0.27 ± 0.01 μm for *FOS* (n = 32 alleles), 0.32 ± 0.01 μm for *NR4A1* (n = 27 alleles), 0.26 ± 0.01 μm for immunopositive BRD4 (n = 47 spots) and 0.26 ± 0.00 μm for immunopositive H4ac (n = 59 spots). As a result, the sum of radii was 0.53 μm (0.27 + 0.26 μm) for *FOS* and BRD4, 0.58 μm (0.32 + 0.26 μm) for *NR4A1* and BRD4, and 0.53 μm (0.27 + 0.26 μm) for *FOS* and H4ac.

Time delay of appearance and disappearance of long residence CREB spots colocalized with CBP spots (>0.6 s) was calculated from the residence time of each spot, although the order of dissociation between these spots may be unclear as it is possible that colocalized signals are quenching.

Statistical analysis

Statistical analyses were done by Origin 2021 or R software (x64 version 3.5.1) software. In comparison between the two distribution, Kolmogorov-Smirnov test was performed. A comparison between the two groups was performed with the Mann-Whitney U test. For comparison among more than three groups, Kruskal-Wallis ANOVA with Dunn's post hoc test or one-way ANOVA with Tukey-Kramer post hoc test was used. For pairwise comparisons, Chi-square test was performed. For comparison against theoretical mean, one-sample t test was done. In all statistics, $p < 0.05$ was considered significant. Bar graphs and scatterplots show mean values and error bars show SEM. In, all box-and-whiskers plots, boxes indicate 25–75% quantiles and the median line, whiskers indicate 10–90% quantiles and squares indicate the mean.